Corso di Laurea specialistica
(ordinamento ex D.M. 270/2004)
in Scienza dei Materiali

Tesi di Laurea

Defects related cathodoluminescence of N-doped silica thin films prepared by RF magnetron sputtering

Relatore
Prof. Francesco Gonella

Correlatori
Prof. Giuseppe Pezzotti
Dr. Enrico Trave

Laureando
Marco Boffelli
(matricola 812427)

A.A. 2011/2012

"Il più solido piacere di questa vita
è il piacere vano delle illusioni."

Giacomo Leopardi

Table of contents

Abstract

Optoelectronic and photonics materials are commonly affected by a large concentration of point defects, which lower dramatically their performances. A strict control on the defects contents and location is necessary. A reliable spectroscopic approach, among the high-resolution probe techniques, which enables to get information on the point defects is the Scanning Electron Microscopy (SEM) coupled with a Cathodoluminescence (CL) spectroscopy. The main aim of the present dissertation is at obtaining, through a detailed cathodoluminescence investigation, a much better understanding of the physical-chemical behaviour of the network in the N-modified structure of silica glass compared to the original silica structure. SiO_2 and N-doped SiO_2 thin films were prepared by radio frequency magnetron sputtering (RFMS) which has proved to be a very suitable synthesis technique for the purpose of this work. Samples were annealed after the deposition, for 1h in air atmosphere, at temperature values from 50°C to 1200°C, with 50°C steps. CL spectroscopy has been used to locally study the nature of lattice defects, in combination with other physical characterizations (i.e., Rutherford back-scattering spectrometry (RBS), X-ray photoelectron spectroscopy (XPS), and ion beam induced luminescence (IBIL)), which helped to quantify the exact amount of nitrogen incorporated in the system.

Introduction

During the last decades, there has been a continuous trend towards the improvement of devices based on materials in different high technology fields of science. Nowadays, commercial devices require the development of tailored materials, with suitable functional properties, for achieving the best performances in photonic as well in optoeletctronic fields. Glassy materials, that have been used for decades in optical applications, are now playing a significative role in the above mentioned fields, even if the lack of effcient approaches to evaluate the physical and chemical properties of their structures produces an inevitable industrial delay in the devices improvement. Moreover, with the trend to continuous aggressive scaling of the components down to 100 nm of size, it becomes necessary to deal with the spatial resolution problem. For the advance in such applications, the locally investigation of the electronic properties in new glass materials is therefore a key issue.

Optoelectronic and photonics materials are commonly affected by a large concentration of point defects, which lower dramatically their performances, even if when properly controlled they can also be viewed as an improving factor. A strict control on the defects contents and location is necessary, but this is -at least partially- out of control, also because their behaviour in the material structure is still rather unclear. However, despite the constant efforts to improve experimental techniques for probing the defects properties, the lack of an "easy" spectroscopical approach forces the material designers to trust unconditionally the computer simulations. The investigation of the materials properties require therefore innovative or improved techniques, alternative to

the standard macroscopic characterization methods. As a matter of fact, it is expected that these requirements can be satisfied by optical methods, by which it is possible to study the electronic properties of defects in a solid materials on the basis of their luminescence features. A much reliable spectroscopic approach, among the high-resolution probe techniques, which enables to get fundamental information on both the nature and the local spatial distribution of point defects is the Scanning Electron Microscopy (SEM) coupled with a Cathodoluminescence (CL) spectroscopy, with detector highly resolved in its spatial and spectral resolution. Cathodoluminescence, which is the light emitted from a sample upon irradiation by an electron beam, may bring about a significant piece of information also on crystal structure, chemical composition and internal stress fields. Henceforth, this equipment, when running at a low electron acceleration voltage, appears as one of the most suitable candidate in characterizations of defect populations in both crystalline and amorphous structures. The CL instrumentation, properly calibrated, can be extremely reliable, being also non-intrusive, very flexible in scanning and, as previously mentioned, highly spatially resolved.

The main aim of the present dissertation is at obtaining, through a detailed cathodoluminescence investigation, a much better understanding of the physical-chemical behaviour of the network in the N-modified structure of silica glass compared to the original silica structure. In this study CL spectroscopy has been used to locally study the nature of lattice defects populations in amorphous SiO_2 and N-doped SiO_2 thin films prepared by radio frequency magnetron sputtering (RFMS), attempting to extend the knowledge of the properties of this material. The incorporation of nitrogen in glassy silica (a-SiO_2:N) has drawn much interest in the scientific community as one promising materials for various applications. In recent years, a large number of scientific papers, regarding the use of this system, have been carried out, aiming at providing a good alternative to amorphous silica, overcoming its limitations. From a chemical point of view, doping SiO_2 structure with nitrogen can lead to the formation of oxynitride (i.e, SiO_xN_y or SiON) compounds. In optoelectronics devices there are many advantages to replacing silicon dioxide with silicon oxynitride, since this material combines the properties of SiO_2,

such as low density of surface states and the high band-gap, with those of Si3N4, that has high atomic density and dielectric permittivity. In particular, the technological importance of silicon oxynitride arises from the tunability of the energy of the band gap (from 5 to 9 eV), simply modifying the stoichiometry. Changing the chemical composition of oxygen and nitrogen, it is possible to obtain unique optical and electronic properties, intermediate from silicon oxide and silicon nitride. For instance, the refractive index (n) can be varied from 1.47 (SiO_2) to 2.3 (Si_3N_4), the dielectric constant (ε_0) from 3.9 (SiO_2) to 7.8 (Si_3N_4) and the residual stress can be switched from compressive to tensile mode. The incorporation of nitrogen can also lead to a fundamental advantage in the removal of silicon dangling bonds from the silica structure, which is one of the reasons of the degradation of electrical properties. This topic is fundamental especially in microelectronics devices in which the neutral and charged electronic defects can determine the electronic performance of a dielectric film.

The RFMS film deposition has proved to be a very suitable synthesis technique for the purpose of this work because, through the possibility of a strict control of deposition parameters, homogeneous and stoichiometric SiO_2-N films can be obtained, free of contaminations, by modifying the system with small amounts of nitrogen in different concentrations. Since the presence of nitrogen atoms in the amorphous host structure can create oxygen deficient centres (ODC) and non-bridging oxygen hole centres (NBOHC), the main challenge is then to relate, by means CL spectroscopy, the variation in type and concentration of these peculiar defects to the amount of the dopant nitrogen in the matrix. Furthermore, by performing different heat treatments on the film samples, it is also possible to follow the evolution of the same system at different temperatures. For this latter purpose, samples were annealed after the deposition, for 1h in air atmosphere, at temperature values from 50°C to 1200°C, with 50°C steps.

In combination with other physical characterizations (i.e., Rutherford back-scattering spectrometry (RBS), X-ray photoelectron spectroscopy (XPS), and ion beam induced luminescence (IBIL)), which helped to quantify the

exact amount of nitrogen incorporated in the system, CL spectroscopy proved capable to provide so far missing information on a nanometre scale regarding the nature, the interrelations and the topological locations of different types of lattice defects in the SiO_2 glass.

Chapter 1

Silicon oxynitride applications

The flexibility of the silicon oxynitride (SiON) properties such the refraction index and chemical resistance allow the usage of this material in the photovoltaic technology and the graded-index optic. Next subsections report Two different applications of SiON showing its technological importance and versatility.

1.1 SiON in photovoltaic (PV) modules

While the bulk materials for PV modules has been subject of an exhaustive review, the dielectric thin films used for the front surface coating is still not studied in detail [1]. The material for the front coating can affect the performance of a bulk silicon solar cell device since it could play a role not only in the optical behaviour, but also in the electronic properties of the devices. The requisite properties depend on the cell design and they are crucial for obtaining increased efficiency of the solar cell. The figure shows the typical configuration of a buried contact (i.e. BC) cell, developed at the University of New South Wales during the mid-1980s [2]. The required properties for the coating of the cell are discussed.
The chosen dielectric thin film must have some characteristic feature to be used as: an anti-reflective (i.e. AR) coating, reducing reflection losses by the surface [3], a film providing surface passivation in order to bond the disrupted

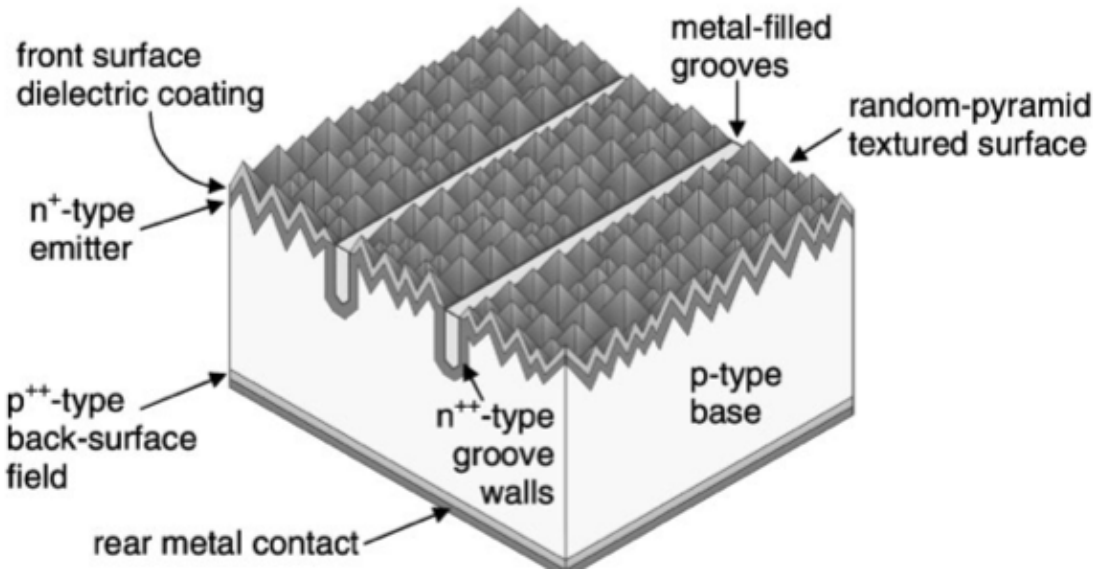

Figure 1.1: *Schematic representation of a BC solar cell.*

silicon lattice at the surface, a mask to facilitate selective metal electroless planting step, a diffusion barrier to achieve emitter diffusion [4]. Also, the coating has to exhibit an excellent chemical resistance, good stability during high temperature processing and, not to interfere with the light passing through the layer, the film should be amorphous and relatively porous.

The first point is one of the most important, because for improving the efficiency of the solar cell the optical losses by reflectance and absorption should be as low as possible in the whole spectrum range. Therefore, cover the surface with a single layer (SLAR) or double layer (DLAR) anti-reflection thin film is essential to obtain the highest possible current generated from the devices. DLAR used for high-efficiency solar cells presents two advantages: the spectral reflectance is lower and the optical performance is less sensitive to the thickness compared with SLAR [5,6]. The improvements due to this double layer occur in the visible and in the near-IR part of the light spectrum.
An example of DLAR configuration in a BC solar cell is given in figure 1.2. The most common coatings that satisfy this feature are silicon dioxide and titanium dioxide that have been extensively used in the past decades.

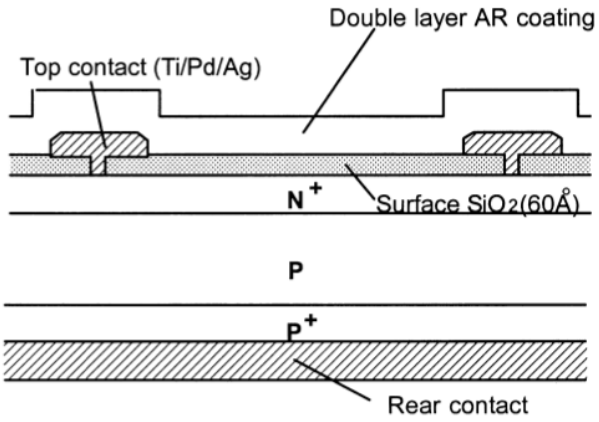

Figure 1.2: *Cross section of DLAR configuration in a BC solar cell.*

Except these, few materials can be used successfully for surface coatings that are: cerium dioxide (CeO_2), silicon nitride (Si_3N_4), hydrogenated silicon nitride (a-SiN_x:H) and silicon oxynitride (SiO_xN_y)[7].

Thermally grown silicon dioxide is used in the bulk silicon solar cell for several reasons, on one hand because it provides an excellent passivation of the silicon surface, whereby terminates the silicon dangling bonds at the surface [8,9], on the other because it possesses great chemical resistance to the majority of acids and base, except HF. At the same time, silicon dioxide

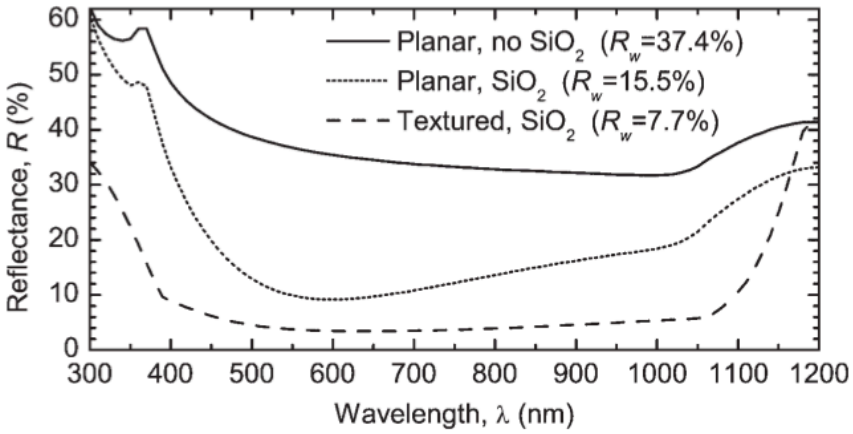

Figure 1.3: *Reflectance spectra of a bare, SiO_2-coated planar silicon wafer, and a SiO_2-coated textured silicon wafer.*

presents some disadvantages such as the low refractive index (n=1.46) that is not suitable to act as AR coating. Figure 1.3 shows the comparison of reflectance achieved with an optimized (textured) SiO_2 SLAR coating, with planar SiO_2 coating and with planar silicon surface. For planar and textured SiO_2 coated silicon wafer the average reflectance is respectively R_w=15.5% and R_w=7.7%, and it should be noted that SiO_2 is not absorbing in the range from 300-1200 nm.

A strategy to overcome these limitations and improve the quality of the layer is replacing the SiO_2 layer with silicon oxynitride because it combines the advantage of SiO_2 with the properties of Si_3N_4 that have a higher refractive index (n=2.2) and a better chemical and mechanical resistance. Also, SiO_xN_y have an increased concentration of nitrogen at the silicon surface, which reduce the concentration of silicon dangling bonds and strained silicon-oxygen bond [3]. These films typically present a variable nitrogen-oxygen ratio, so it is possible to obtain an intermediate value of refraction index varying the composition. Figure 1.4 shows the values of refractive index of SiO_xN_y films with different composition. The refractive index of silicon oxynitride varying from 2.05 to 1.45, if an average composition (i.e., SiO_2N_2) is considered, the refraction index is in the range of 1.80-1.88 [10,11]. Besides these properties, this material can be chosen for surface coatings for its increased resistance to acids and base, including HF. Silicon oxynitride has shown improved performance as a diffusion barrier, thus is less permeable to diffusing species and, the low surface state density is maintained [12].

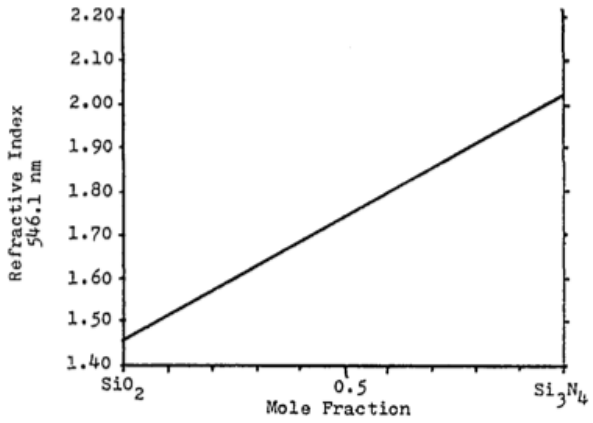

Figure 1.4: *Refractive index range from SiO_2 to Si_3N_4.*

1.2 SiON in optoelectronic devices

Optoelectronics is considered one of the most important fields for the development of next-generation technology. From the 1965 when Gordon Moore, the cofounder of Intel corporation, made his prediction [13], is becoming clear that a new way would have been needed to overcome the limitations of integrated electronic technologies. The so-called Moore's law that has been proven accurately during the last decades state that the number of transistors in an integrated circuit would double every two years approximately. In fact as a circuit gets smaller, difficulties arise from the heat dissipation and current leakage, degrading the properties of the semiconductor and affecting the ability of electronic circuits to transfer the information. Substituting electron with photon, i.e. developing a technology that can manipulate them, is one of the best way to overcome this limitation [14]. Since that silicon is still the leading material for electronic application, integration of optical properties in silicon technology is necessary for development of new optoelectronic devices. The basics of silicon photonics have been studied since the mid 1980s, but only in the recent year a consistent number of problems were overcome [15].

Optical integration based on silicon technology can combine signal splitting switching and amplification, that are fundamental in the optical transmission of a signal and could bring new functionalities to electronic components such as low propagation losses, immunity to electromagnetic noise and high bandwidth [16]. One of the problems for the practical reliability of the optical integration is that, differently from the electronic system where all the components are built on a single material, the photonics components are usually incompatible with silicon. For instance, one of the approaches is based on hybrid technology where Silicon, Germanium and other III-IV semiconductor are integrated together. Instead, using silicon based material such as silicon dioxide, nitride and oxynitride could lead many advantages for the fabrication technologies.

1.2.1 Silicon oxynitride waveguides

One of the fundamental components in integrated optical circuits is the waveguide, which permits the connection among the various devices. The waveguide that are simply a system in which electromagnetic waves can be confined and manipulated, can be divided in many different kinds, mainly depending on their geometry constructions. Normally a glass or a dielectric material (core) is cladded by other material, which have a refraction index different to the first. The main requirements for glass or dielectric waveguides are the lowest possible optical absorption that implies a low energy loss during the propagation. Generally, the absorption losses are due to molecular bond or point defects in the core layer. Therefore, the chosen material for the waveguide core determines the wavelength of the signal and the intrinsic losses. A good choice is to consider materials already used in microelectronics that could have a good compatibility with silicon layer: silicon oxynitride (SiO_xN_y), silicon nitride (Si_3N_4) or Si nanoparticles embedded in silica layer (SiO_2 Si-rich) are the most attractive dielectrics for this purpose.

Several effort were made by researchers the mid-1990s to describe these new systems [17]. Among that material, SiON is particularly suitable for optical integrated circuit for the tunability of its refractive index, its transparency and its low absorption losses over a wide wavelength range (from UV to IR) [18]. One of the pioneering study on SiON as a material for waveguides was reported in 1972 by R.J. Rand and R.D Standley which described for the first time the properties of a CVD SiON film on a fused silica substrate [19]. Just in the 1998 a group from University of Twente studied in detail this system, also creating the design of the waveguides for optical communication transmissions [16,20]. The simplified waveguide structure, fabricated on a thermally oxidized silicon wafer, is shown in fig 1.5 (a). The silica cladding layer and the oxynitride core were both realized by PECVD deposition, but for compensate the birefringence, a Si_3N_4 layer deposited by LPCVD was added. Figure 1.5 (b) shown the SEM micrograph of the waveguide.

The channel losses, one of the most important features for optical transmissions, were measured to be below 0.1 dB/cm at 1550 nm. The removal of hydrogen (added by the chemical precursor in PECVD process) for achieving low propagation loss were made by annealing thermal treatments up to 1100°C, which could induce side-effect like significant interlayer diffusion and microcracks resulting in the deterioration of the devices.
For this reason, this system was subsequently improved by doping the SiON

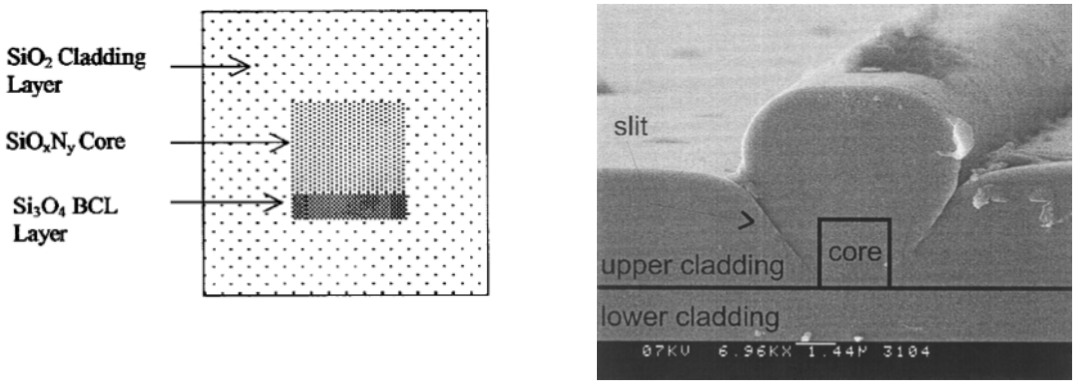

(a) (b)

Figure 1.5: *(a) cross-section of a waveguide structure using silicon oxynitride and (b) SEM micrograph of the complete structure.*

core with boron and phosphorus to permit annealing treatments at the lowest temperature [21]. Another method to reduce the hydrogen amount is optimizing the PECVD process, as reported in [22].
In order to obtain also a low stress distribution, authors report the architecture of this strip-loaded waveguides (illustrated schematically in figure 1.6), typically used as a microcavity resonator.

An alternative approach to reduce hydrogen concentration and to have a better control of the deposition parameters is to use another method of film deposition, namely the radio frequency magnetron sputtering. This technique, widely used in microelectronics and in photonics, was applied to oxynitride waveguides for the first time in 1990 by Del Giudice et al., which demonstrates the possibility to obtain silicon oxynitride waveguides, without hydrogen, with a tunable core index [23].

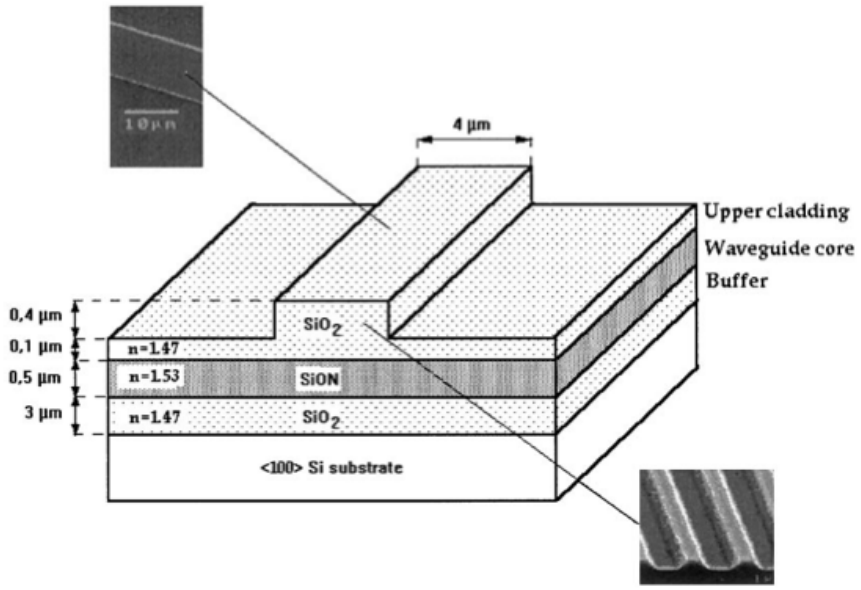

Figure 1.6: *Structure of single-mode strip-loaded oxynitride waveguide.*

1.3.4 Other optical devices based on Silicon oxynitride

The large flexibility of silicon oxynitride combined with its excellent optical properties makes this material one of the candidates for the fabrication of waveguides used in several different optical devices such an electro-optic modulators, second harmonic generator and micro-electrical mechanical systems (MEMS) [16,24]. These devices are the fundamental components in optical integrate circuits through which is possible manipulate electromagnetic wave, amplifying, duplicating or switching them.

An interesting application is using silicon oxynitride as a constituent in non-linear Mach Zehnder interferometers (MZI), which can operate as an opto-optical switch. This system, realized by Driessen et al., is able to integrate the linear and non-linear waveguides. This is possible choosing the same refractive index for the oxynitride cladding and the non-linear waveguides, formed by a polymer [25]. A schematic section of this structure is given in figure 1.7. Another application is using SiON waveguides in the micro-cavity resonator devices that can be used as channel dropped filter in waveguides division multiplexing (WDM) systems [26].

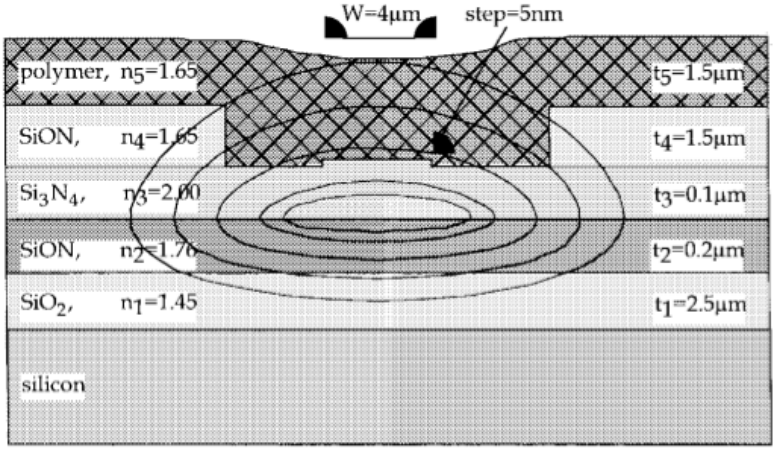

Figure 1.6: *Structure of non-linear MFI using silicon oxynitride.*

These are only few applications in which this material can take place, and it was possible to demonstrate on one hand how this material can serve as "general" waveguides, on the other, how it is used as "special" waveguides in a great variety of devices.

Chapter 2

Silicon oxynitride and theory of defects

2.1 Structure of crystalline and amorphous silicon oxynitride

The physical and the electro-optical properties of Silicon oxynitride films depend on their chemical composition, electronic structure and morphology; thus a deep understanding of the material structure is necessary for the development and fabrication of oxynitride based opto-electronic devices. The study of the relation between the structure and the chemical composition could help to understand the effect of the bonding structure on the electrical and optical behaviour of these materials. Also, knowing the local structure is fundamental to describe the defect of the material, which are the first cause for the degradation of these properties.

2.1.1 Crystalline structure

While the composition of amorphous silicon oxynitride can continuously vary between SiO_2 and Si_3N_4, the only known crystalline form is Si_2N_2O which is considered a stable intermediate phase. The equilibrium of silicon oxynitride can be expressed in two ways: by nitration of a solid mixture composed by silicon oxide and silicon in a temperature range of 1420-1500 °C, (2.1) or by direct nitration of solid SiO_2 (2.2) as described by the following reactions [27]:

$$3\ Si_{(s)} + SiO_{2\,(s)} + 2\ N_{2\,(g)} \rightarrow 2\ Si_2N_2O_{(s)} \qquad (2.1)$$

$$4\ SiO_{2\ (s)} + 2\ N_{2\ (g)} \rightarrow 2\ Si_2N_2O_{\ (s)} + 3\ O_{2\ (g)} \tag{2.2}$$

The perfect crystalline phase of Si_2N_2O can serve on one hand for a direct comparison of the structural properties with perfect SiO_2 and Si_3N_4, on the other as a reference system in the study of real polycrystalline or amorphous forms. The comparison between this phase and their structural parameters, reported in [28] are summarized in table 1.

Crystal	α-Si_3N_4	β-Si_3N_4	α-SiO_2	Si_2N_2O
Lattice constant (Å)				
a:	7.766	7.586	4.913	8.843
b:				5.437
c:	5.615	2.902	5.405	4.835
Space group	Hexagonal C_{3v}^4	Hexagonal C_{6h}^2	Hexagonal D_3^4	Orthorhombic C_{2v}^{12}
Formula unit *Z*	2	4	3	4
Bond distance (Å)				
Si—N (average)	1.738	1.730		1.714
Si—O (average)			1.610	1.623
Bond angle				
Si—N—Si	118.8	119.9		120
Si—O—Si			144	147.4
Effective charge Q^* in electron				
Si	1.48(0.85)	1.50(0.86)	1.40(0.81)	1.46(0.84)
N	6.89(1.12)	6.87(1.13)		6.90(1.10)
O			7.30(1.02)	7.25(1.01)

Table 1: *Structural properties of SiO_2, SiO_2N_2 and Si_3N_4.*

Figure 2.1 compares the atomic structure of silicon dioxide and silicon oxynitride. Silicon nitride exists in 2 polymorphs, α-Si_3N_4 and the stablest form β-Si_3N_4, silicon dioxide can form several polymorphic structures, some stable and some metastable. In the common α-quartz and in β nitride, silicon is bonded to four oxygen atoms at an average distance of 1.61 Å, and 1.74 Å, respectively. Indeed, in oxynitride form, the bond length of Si-O is longer than in silicon dioxide and the bonding angle between Si-O-Si become larger.
Crystalline silica and silicon nitride form a continuos series of solid solutions formed by the polymorphs of the exceeding component, and silicon oxynitride.

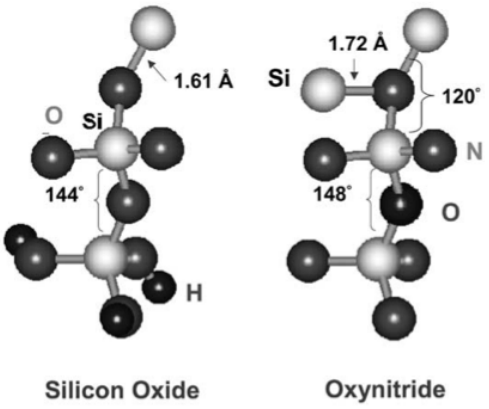

Figure 2.1 : *Representation of silicon oxide and oxynitride structure.*

The binary phase diagram, that show the thermodynamic relation between temperature and composition of the system SiO_2-Si_3N_4, without the gas phase,reported by Hillert et al. [29] is shown in fig 2.2.

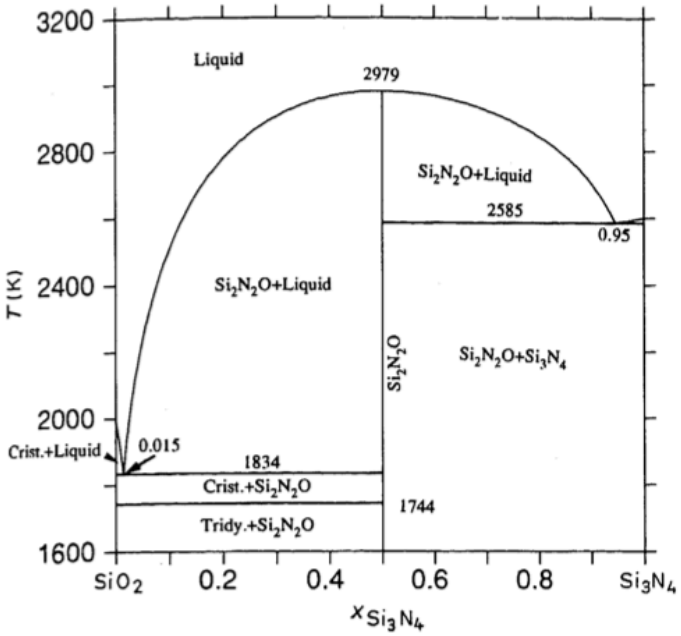

Figure 2.2 : *SiO_2-Si_3N_4 phase diagram.*

2.1.2 Amorphous SiO_xN_y

Amorphous silicon oxynitrides are expected to be in a non-stoichiometric form, silicon rich with a variable amount of nitrogen and oxygen. Depending on the relative presence of the different atom's structure may consist of Si-O, Si-Si and Si-N bonds.

The coordination number of the cations in the vitreous network is the most basic element for modelling the amorphous structure. Since the silicon is fourfold coordinated in both silica and silicon nitride, amorphous oxynitride films are expected to show a tetrahedral coordination of neighbour atoms around silicon. However, the short range order that express the order at a short distance between the atoms which occupy the sites in the network, in tetrahedral solids such SiO_2, α-Si_3N_4, β-Si_3N_4 and crystalline Si_2N_2O is described by the Mott rule:

$$N_c = 8 - n \tag{2.3}$$

where N_c is the coordination number, and n is the number of the electrons valence. Following this rule Si atom has 4 valence electrons ($3s^2 3p^2$), O atom has 6 valence electrons ($2s^2 2p^4$) N atom has 5 valence electrons ($2s^2 2p^3$), and their coordination number are 4, 3 or 2 respectively. This implies that in SiO_2 and in Si_2N_2O each O atom is twofold coordinated with Si atom, and similarly each N atom in Si_3N_4 and Si_2N_2O is threefold coordinated.

Thus, theoretically, amorphous silicon oxynitride, a-SiO_xN_y, of different composition are composed by the mixture of Si-N bonds and Si-O bonds and involves five types of different tetrahedra $SiO_\nu N_{4-\nu}$ (ν = 0, 1, 2, 3, 4 for composition x,y) with distribution given by random statistics [30]:

$$w(\nu,x,y) = \left(\frac{2x}{2x+3y}\right)^{\nu}\left(\frac{3y}{2x+3y}\right)^{4-\nu}\frac{4!}{\nu!(4-\nu)!} \tag{2.4}$$

This relation expresses the relative probability of the five different types of tetrahedrons in an amorphous silicon oxynitride film. The distribution function can be determined replacing the x and y, with the amounts obtained from

characterization techniques, such RBS or XPS. Has been observed that silicon oxynitride films are formed by 40% of SiO_3N tetrahedra, and as the N content decrease as the number of SiO_3N and SiO_2N_2 decrease, with an increase in the number of SiO_4 tetrahedrons [31].

Considering a perfect chemical order, where only Si-O and Si-N bonds are present in silicon oxynitride, a simulation of the amorphous network model (figure 2.3) can be done on the basis of density functional theory (DFT) methods [32].

So far we have considered the amorphous silicon oxynitride as formed only by Si-O and Si-N bonds, but the real structure can involve also Si-Si bonds and some atoms not fully coordinated. This behaviour cause a deviation of the Mott rule (1.1) by up to 5% [30].

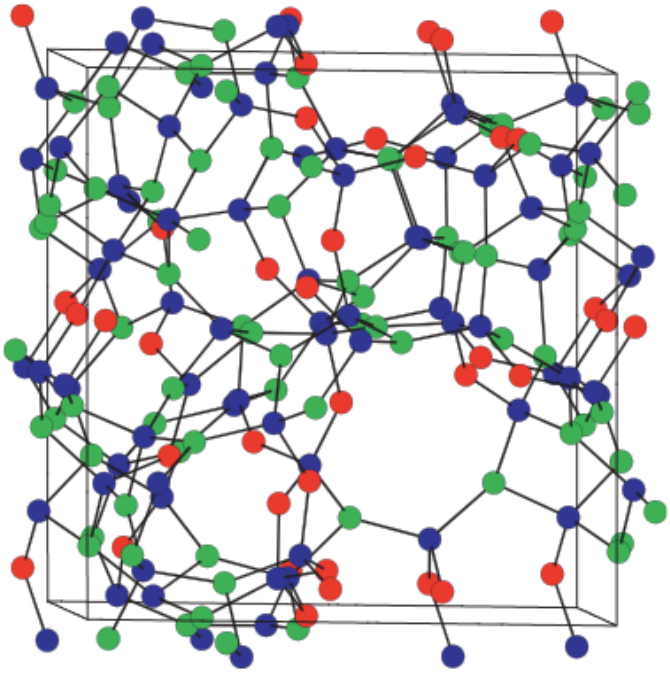

Figure 2.3 : *Representation of silicon oxynitride amorphous structure.*

2.2 Theory of point defects

The quality of a dielectric film is governed by the neutral and charged electronic defects; indeed their presence in the matrix can dramatically change its optical, electrical and structural properties. There are many factors that may lead to the formation of defects in the matrix or the transformation of existing defects in another type of defect, such as manufacturing process, mechanical stress, change of temperature and presence of impurities.
Generally the defects in a solid matrix can be divided according to their dimension as point defects, linear defects (dislocation) and plane defects. The point defects, on which is focused this study, occurs only in a single lattice point influencing the surrounding atoms and can be grouped in intrinsic and extrinsic defects. Intrinsic point defects involve only atoms of the matrix while extrinsic point defect involve different atoms from the host lattice, such as those are used for doping. As for the intrinsic defects, there are two different arrangements that may occur in the lattice, called Frenkel and Schottky defects which are illustrated in figure 2.4 for an ionic crystal.

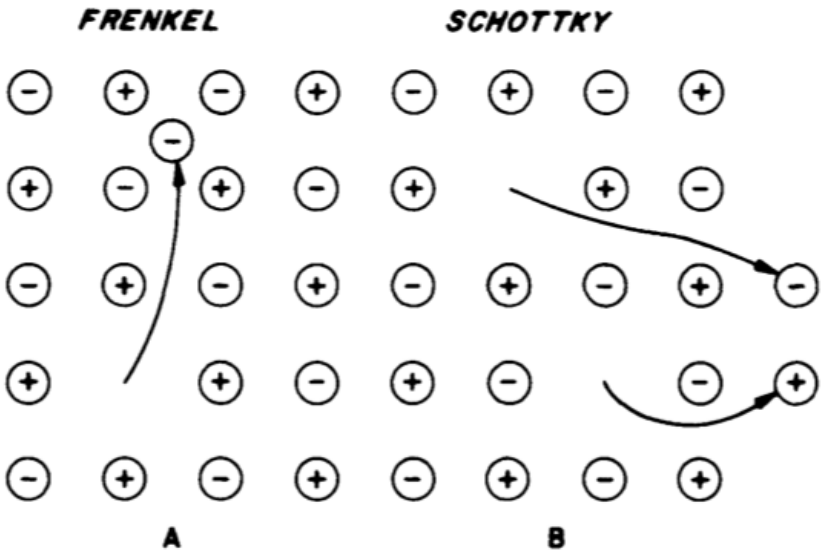

Figure 2.4 : *Schematic illustration of Frenkel and Schottky point defects.*

The Frenkel defects consist in an ion displaced from its place in the elementary cell to a position where normally there are no atoms, namely an interstitial site. This generates a pair of defects: a vacancy and an interstitial atom, which can have positive or negative charge according to anion or cation displacement. Instead, a Schottky defect consists of a pair of vacancies without interstitial atom which is formed by removing a pair of oppositely charged ions.
The importance of the vacancies created by both mechanism is due to its ability to trap electrons displaced from ions when an energetic radiation interacting with the system. Simply the electron trap centre occurs when an electron is present in a location where normally is not found, on the contrary a hole trap centre occurs when electron is missing from its normal position.

Normally, in ideal crystal, a displaced electron return rapidly to its original or similar ion, but if a Schottky or Frenkel defect is present the electron could be trapped in a stable configuration, forming a F centre. Considering the band theory these processes involve the excitation of an electron from the valence band into the conduction band, and its relaxation to a stable level formed by the vacancy. An example is by the halide vacancy trap, as illustrated schematically in figure 2.5.

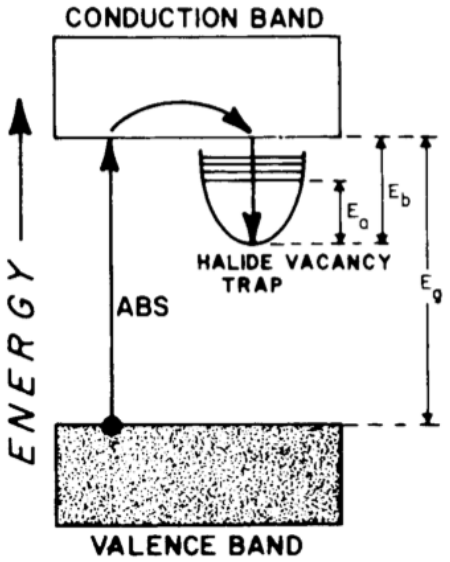

Figure 2.5 : *Halide vacancy trap in band gap materials.*

At the vacancy, the electron is trapped by the positive charge of the surrounding atoms. This creates additional energy level between the vacancy and the conduction band, which may cause the light absorption. As well a vacancy surrounded by negatively charged atoms can act as hole traps [33].

2.2.1 Intrinsic and extrinsic defects in silicon dioxide and oxynitride

Defects in amorphous silicon oxynitride glass include intrinsic defects, due to point defects of the silica host matrix, and extrinsic defects caused by the presence of nitrogen as a dopant, or to excess or deficiency of oxygen.
In pure silicon dioxide amorphous structure, the intrinsic defects includes oxygen or silicon vacancies and their interstitial or under-coordinated silicon and Si-Si and O-O homobond. However in oxynitride, there are a more complex network in which the silicon can bonds randomly with both nitrogen or oxygen atoms. In these networks, defects are electrostatically neutral but may become positively or negatively charge by trapping respectively holes or electrons. It is possible to distinguish charged, or uncharged defects and, without considering their electrical charges, they can be grouped in diamagnetic and paramagnetic. In general all paramagnetic defects have an associated optical absorption band since they represent half-occupied energy transition to the valence or to the electron band, while the diamagnetic defects may have absorption band due to the electronic transition to the conduction band. However, not necessarily this absorption transition are accompanied by a radiative relaxation [34].

Many type of defects has been extensively discussed in literature, which has been found experimentally or by computational approach. Defects structure in amorphous solids have been investigated by several spectroscopic techniques including electron spin resonance (ESR), photoluminescence spectroscopy (PL), photoluminescence excitation spectroscopy (PLE), cathodoluminescence spectroscopy (CL), infrared spectroscopy (IR) and many more. Nowadays several type of known defects exists in silica materials, even if its nature and correlated properties are not completely understood. Native intrinsic and extrinsic defects in amorphous or crystalline silica are associate to deficiency or excess of oxygen [35].

By computational approach, using quantum-mechanical calculation, is possible to obtain a detailed description of the defects structures based on the experimental data collected. This represent an indispensable tool to study the nature and the optical properties of defects, as well as the spectroscopical approach to characterize the material. Calculations obtained through a molecular dynamic approach for pure silica, provides the expected absorption band for the oxygen excess or deficiency associated defects, as shown in figure 2.6.

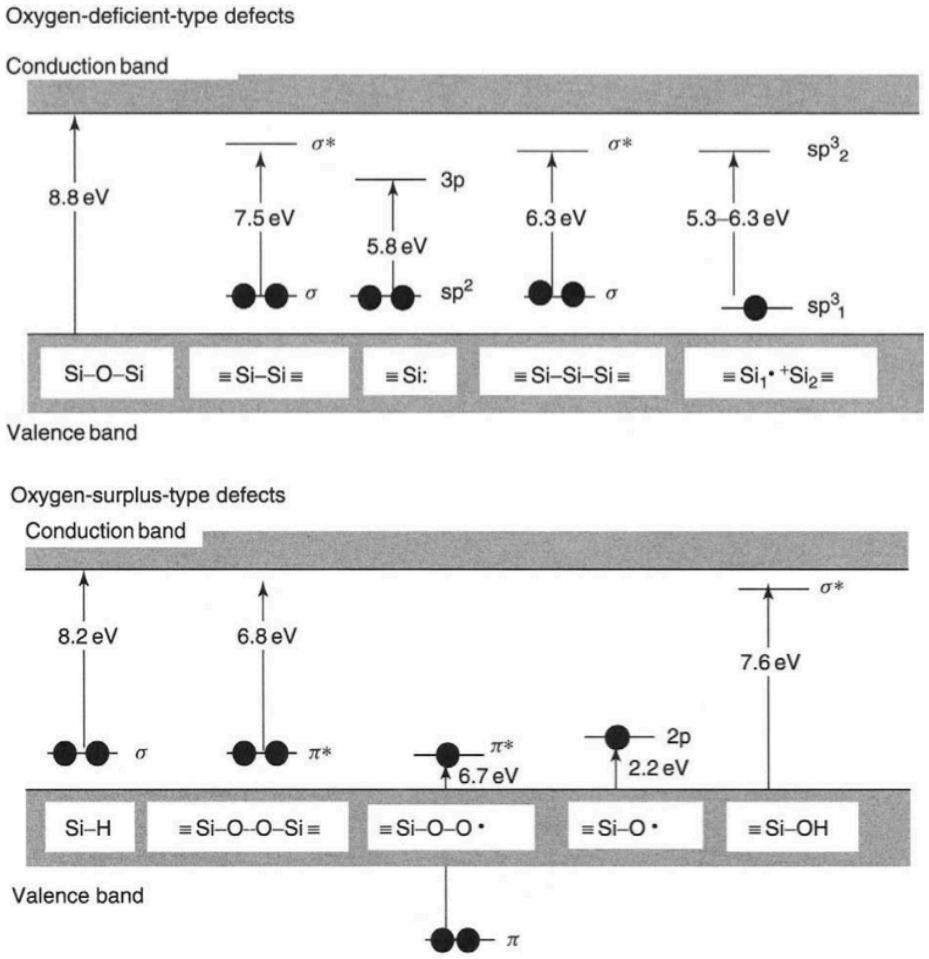

Figure 2.6 : *Oxygen excess and deficiencies defects associated absorption.*

Chapter 3

Deposition and characterization techniques

3.1 Physical vapour deposition process

Physical vapor deposition (PVD) is a general term to describe several atomistic deposition processes in which the vaporization of a material, from a liquid or solid source in the form of atoms or molecules occurs through a low pressure gaseous or plasma environment, and a deposited layer is formed on a substrate where the material condenses. This kind of processes is commonly used for the fabrication of thin films of elements, alloys and compounds, with thickness in the range of a few nanometers to micrometers. PVD processes can be distinguish in several different methods of deposition, among which we can mention: evaporative deposition, electron beam PVD, sputter deposition, cathodic arc deposition, pulsed laser deposition. Sputter deposition is used extensively in the optoelectronic and photonic industry, due to its capacity to deposit the highest melting point and dielectric materials. This technique is one of the main processes of manufacturing optical waveguides, anti reflection and low emissivity coating on glass. For these reasons, the N-doped SiO_2 thin films investigated in the present dissertation were fabricate using a sputter deposition in a RF magnetron configuration. The following subsection explains the experimental configuration of this deposition method, while in appendix A is reported a complete description of the sputtering process.

3.1.1 DC magnetron sputtering

In the magnetron sputtering technique, the DC diode configuration is implemented by means of two magnets placed on the cathode in order to lengthen the electron trajectory before the collision with the anode. The secondary electrons affected by the magnetic field, may be deflect to stay near the target surface and, by a suitable configuration of the magnets, can be made circulate on a closed path. This high flux of electrons creates a high density plasma from which a high flux of ions that sputter the target material is developed.

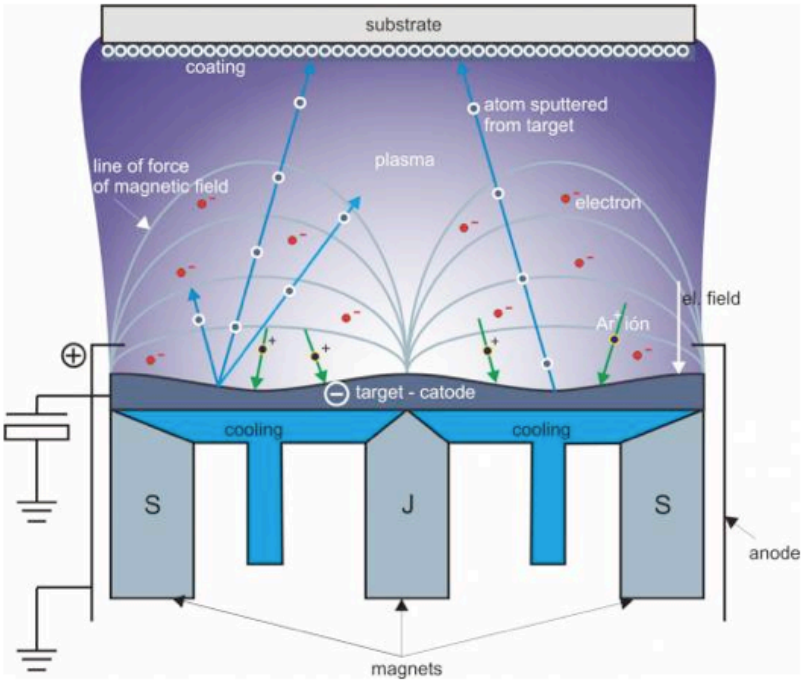

Figure 3.1 : *Planar magnetron configuration.*

In comparison with DC diode configuration and other techniques the ion flux developed is two orders of magnitude greater, accompanied by an overall increase of deposition rate. Since the electron path follows the magnetic field line, the target undergoes a non-uniform erosion. Moreover, due to the high number of collisions the target can be overheating, so an efficient cooling

system is needed. The Figure 3.1 illustrate the planar magnetron configuration, that is one of the most used magnetron sputtering sources. This configuration forms a vaporization source that consists of two parallel lines, and the sputter-erosion path have a closed or an elongated circle shape on the planar surface of the target.

3.1.2 Radio-frequency (RF) sputtering

In the radiofrequency sputtering, the DC power supply is replaced by an RF supply in order to be able to use target of dielectric material. The DC diode sputtering does not allow the deposition of insulator because of the buildup of a positive surface charge that prevents the sustaining of the plasma. When the rf potential is coupled to an electrode, an alternating positive and negative potential appears on the surfaces (typically the RF power used for sputter deposition is 13.56 MHz).
During the positive half cycle electrons can reach the electrodes faster than ions, which are collected during the negative half-cycle. The ions current is much smaller than the electrons current and does not balance the collected electron charge causing a positive potential of plasma that faces the electrodes. Since the target is capacitively coupled to the plasma, there are no difference if the target is electrically conductive or insulating because the positive potential is such that accelerating ions with quite energy to cause sputtering. In this configuration, the surface of the target is smaller than the sum of surface area of chamber's wall in order to make on the target a more negative potential than the substrate. This is a necessary condition for the plasma discharge and for accelerating the ions of the working gas to the target.

Rf sputtering present several advantages, among which the high stability and the capacity to fabricate high quality complex system using a deposition rate and power on target as the only parameters to control the growth of the film. One of the disadvantages in RF sputtering of electrically insulator target is that most of this material exhibit poor thermal conductivity, high coefficients of thermal expansion and are usually brittle materials. Since the bombarding ions produce heat on the target, large thermal gradients are generated, and this can result in fracturing the material if high power level is

used. High rate RF sputtering is generally limited to deposition from targets which are not susceptible to thermal shock having a low coefficient of thermal expansion.

3.1.3 Bias sputtering

The morphology and the properties of the thin films can be modified during the deposition by varying the substrate temperature or applying a bias voltage. In the Bias sputtering, the polarization of the substrate is induced in order to provide energy to the film through a mild bombardment caused by the attraction of the ions of the working gas. The bombardment of the substrate during the film growth may involve several effects, among these the increasing of the density, the variation of the internal tension, the increase of the hardness and may also promote diffusion phenomena or chemical reactions.

3.1.4 Reactive sputtering

Through reactive sputtering deposition is possible to synthetize compound films, such as oxide and nitride, by the chemical reaction between the atoms sputtered from an elemental target with a gaseous species opportunely introduced into the vacuum chamber. The gaseous mixture introduced is mainly composed by the inert working gas and the reactive gas, which may be in molecular state, such N_2 or O_2. Varying the relative partial pressure of the two gases in the mixture, the composition of the film can be controlled.

A typical problem that affects the reactive sputtering is the "poisoning" of the target caused by the reaction, or the absorption, of the reactive gas onto the target surface. Poisoning have to be prevented because greatly reduce the sputtering rate and the sputtering efficiency in the case of metallic target. This problem may be controlled having a high sputtering rate, like in the magnetron sputtering, and monitoring the partial pressure of the reactive gas as a function of the reactive gas flow.

3.2 Instrument

The instrument used to fabricate the silicon oxynitride thin films in this dissertation, is a custom-built radiofrequency magnetron sputtering, equipped with 3 RF sources, able to both bias and heat the sample during the film growth. (Material Science Laboratory of the Molecular Science and Nano system Department of the Ca' Foscari University). The needed high vacuum conditions (in the range of 10^{-7} mbar) are obtained through a turbo-molecular pump that is linked with a rotative pump which is used on one hand as a primary pump to reach the necessary pressure (10^{-2} mbar) to activate the turbo-molecular pump, on the other as a backing pump. The instrument is also equipped with a cryogenic pump that serves to improve the vacuum level and to remove the humidity inside the chamber which can affect the film synthesis by the interaction with the hydroxyl group. The vacuum chamber is supplied by a "fast entry" system for the introduction and the extraction of the samples directly inside the chamber without breaking the deposition chamber vacuum conditions. The vacuum level inside the chamber can be monitored by means of two vacuum gauges working at different pressure ranges. The first, a Wide Range Gauge (WRG) system, is constituted by a Pirani vacuum gauge, which works in pressure ranges of $10^{-2} \div 10^{3}$ mbar, and by a Penning vacuum gauge that works in pressure ranges of $10^{-8} \div 10^{-2}$ mbar. The second, normally used during the deposition to regulate the pressure of the working gas, is a capacitive gauge which works in the pressure range of $10^{-4} \div 10^{-1}$ mbar with sensitivity of 1×10^{-4} mbar. As mentioned before the instrument is equipped with three independent radio-frequencies sources which may act on three different targets, with three independent gas lines and with quartz lamp that allows the heating of the substrate up to 500°C. The system can also bias the sample holder during the deposition with an additional RF source.

3.3 Characterization techniques

In the course of this thesis several characterization techniques have been used, such as cathodoluminescence spectroscopy (CL), Rutherford backscattering spectroscopy (RBS), x-ray photoelectron spectroscopy (XPS) and ion beam induced luminescence (IBIL). Since the main technique used for the

characterization of the samples is the CL spectroscopy, its explanation will be given in detail in chapter 3, including a physical background on its principles and a complete description of the instrument.
The descriptions of all the other techniques are reported in appendix. Following are reported the generalities of the instruments through which the measurement were performed.

3.3.1 RBS and IBIL

RBS and IBIL analyses were performed at I.N.F.M Legnaro National laboratories (Italy), using a $^{4}He^{+}$ ion beam at the energy of 2.2 MeV and 1.5 MeV, respectively.

3.3.2 XPS

XPS measurements were performed at the Department of chemical sciences of Padova University, with a Perkin Elmer Φ 5600ci spectrometer equipped with non-monochromatized MgKα (1253.6 eV) and AlKα (1486.6 eV) x-ray sources. To perform the measurement the AlKα radiation, in the 10-7 Pa pressure range was used. Argon ion sputtering, with 3 kV of accelerating potential, was carried out by an ion gun fitted in the analysis chamber in order to record in-depth spectra.

Chapter 4

Introduction to cathodoluminescence spectroscopy

4.1 Introduction

Luminescence is a common process in solid materials, which results from a photon emissive transition in atoms, molecules or lattice from an excited electronic state to a state with lower energy after the excitation of the system. According to the source of excitation, several types of phenomena can be distinguished: photo-, cathodo- and thermo luminescence are only a few of these. Cathodoluminescence (CL) is one of the various processes that result if the sample is irradiated with an electron beam. This phenomenon was observed for the first time during the experiment of electrical discharges in evacuated glass tubes, which showed luminescence when the cathode rays hits the glass. In the last decades, this has been an important technological phenomenon on which were based the cathode ray tubes (CRT) instrument, such a television or computer terminal. With the development and the improvement of the scanning electron microscopy (SEM), cathodoluminescence has emerged as a powerful tool for the characterization of the luminescence properties of materials. Indeed the two techniques can be coupled, originating an CL-SEM apparatus. Other luminescence properties of materials, such as photoluminescence, have been widely studied since that they do not require vacuum chamber and focused electron beam.

4.2 Process of luminescence

The mechanism that implies the photon emissions in inorganic materials are very similar for the different excitation energy; therefore, the comparison of CL with other phenomena such as Photoluminescence and electroluminescence yields similar results. However, many differences arise in the features of the characteristic excitation process; indeed, the excitation with an electron beam normally stimulates every mechanism of luminescence present in a specimen, while the excitation with light beam depends strictly to the energy of the photons and can be used for selective excitation. In particular, irradiating by means of electron beam a solid target, like semiconductor or insulator, may result in the creation of electron-hole pairs, in number several orders of magnitude higher than by optical excitation. So, in this way we could obtain an increased yield of the luminescence process in high band gap materials.
Whatever is the excitation source, the mechanism of luminescence is simply described in terms of three elementary processes: 1) absorption of excitation energy and stimulation of the system into an excited state, 2) transformation and/or transfer of the excitation energy, and 3) emission of light and relaxation of the system to a non-excited state [37]. Upon excitation, an electron could pass from the ground state level to an excited state, and return to the ground state level through radiative transition or without photon emission. If the emission is radiative, the wavelength of emitted photons depends on the energy difference between the ground and excited levels. Normally, in semiconductor or insulator materials this process means the excitation of an electron from the valence band to the conduction band with the generations of a hole, so the luminescence may be produced by a band-band transition.

4.2.1 Intrinsic and extrinsic luminescence

Especially in CL analysis is useful to divide the luminescence transition between intrinsic or fundamental emission, and extrinsic or activated emission [38]. Intrinsic CL is due to recombination of an electron from the conduction band and hole from the valence band across the fundamental energy gap; so it is "intrinsic" properties of the material, and the light are emitted with photons energy of $h\nu=E_g$. This process can take place only in semiconductors and can

be divided in direct and indirect transition. For semiconductor material, in which the maximum of the valence band and the minimum of the conduction band occur at the same values of the wave vector k, the momentum is conserved, and the transition, with a photon emission, is direct; if the maximum and the minimum of the bands do not occur at the same k values, the transition is indirect and to conserve the momentum the recombination of an electron-hole pairs must be accompanied by the simultaneous emission of a photon and a phonon. The first one material is called direct-gap semiconductor (GaAs, InP, CdS) and the second indirect-gap semiconductor (Si, Ge, GaP), as illustrated schematically in figure 4.1. The probability that the indirect transition can occur is very lower in comparison with the direct one; therefore the CL emission of indirect-gap semiconductors is relative weak.

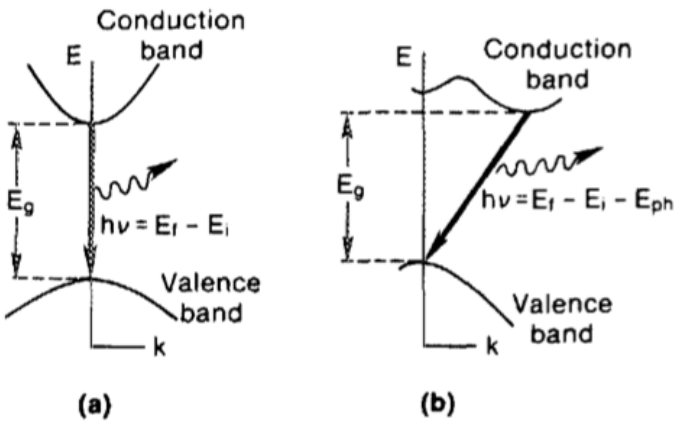

Figure 4.1 : *Representation of transition in (a) direct-gap and (b) indirect-gap semiconductors.*

Extrinsic CL emission takes place in the semiconductor or insulator materials, in which the transition is "activated" by impurity atoms or other defects and occur between localized states within the "forbidden" energy gap. The emitted luminescence is characteristic of the particular activator and can be more intense than intrinsic CL transition. Luminescence centres can be differentiated by their energy position within the energy gap and divided into electron traps near the conduction band (donor level) and recombination sites in the proximity of the valence band (acceptor levels).

We should note that in insulator like silica a high energy gap (9 eV) exists between the conduction band and the valence band, so a precondition for CL process is the existence of activator which form discrete energy levels in the forbidden zone. According on what is explained before, a simplified outline of different transition that lead emission in semiconductor or insulator materials is given in figure 4.2, in which CL due to recombination processes may be due to (a) recombination by direct band-to-band transition (intrinsic CL); (b-e) recombination via localized states in the forbidden gap (extrinsic CL); (f) excitation and recombination within the defect energy levels. Besides these processes, non-radiative recombination of electron-hole pair, as in the case of multiple phonon emission, direct conversion of an electron into heat and recombination due to surface states defects could occur [39].

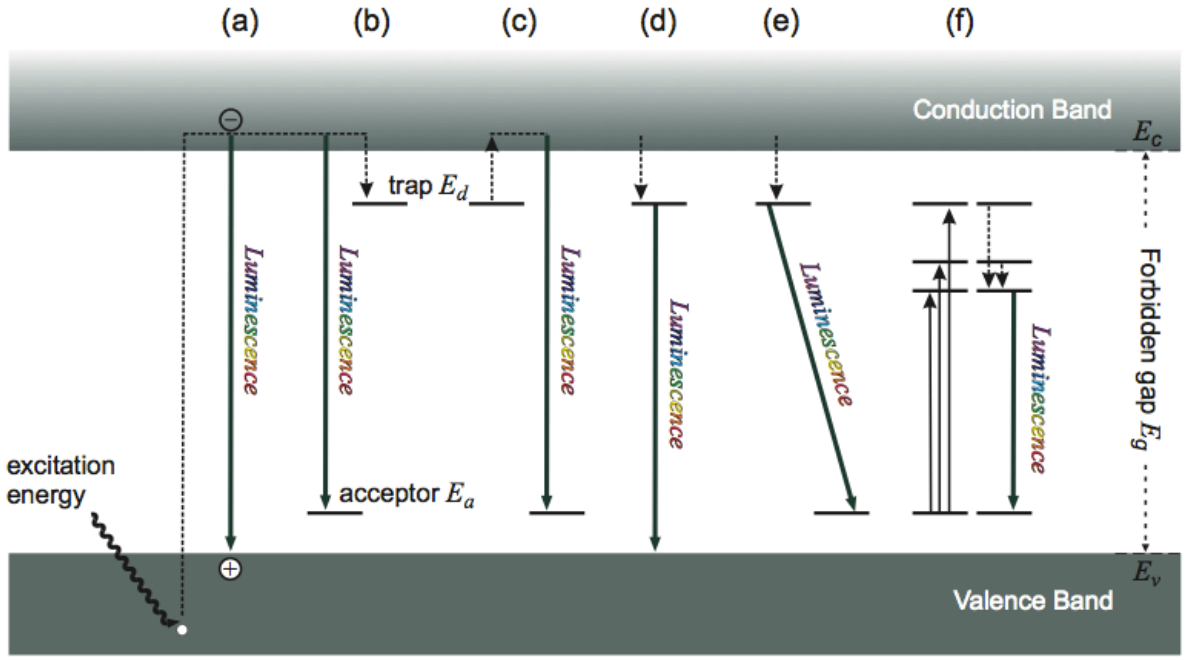

Figure 4.2 : *Luminescent recombination mechanism due to (a) intrinsic CL, (b-e) extrinsic CL and (f) localized states. E_a and E_d are acceptor and donor level, respectively.*

4.2.2 Crystal field theory

To have a better understanding of the mechanism of luminescence, we should consider that the luminescence centre is part of a complex lattice and is strongly influenced by its neighbour atom. The diagram of level could be not sufficient to describe the whole luminescence process, and beside the three basic process it is important to consider the interaction between the center and the surrounding. This influence on the orbital energy is well described by the crystal field theory [40] and lead to a change in the local symmetry of the luminescent centre which result in a splitting of electron energy levels. The excitation and relaxation are separated by a time interval in which the surrounding atoms can shift to a new equilibrium position with a new distance to excited centre. During this process, some of excitation energy is transferred to the crystal lattice, and the emission band results shifted to lower energy (Stoke shift) respect to the absorption band. The stronger the interaction, the bigger are the Stoke shift and the width of the emission line.

The mechanism of excitation and emission of an individual luminescence is well described in the diagram in figure 4.3. This scheme shows the potential energy curves of the absorbing centre as a function of the relative distance R of the nucleus to the equilibrium position (electron in the ground state with vibrational level $n = 0$).
When the system is irradiated with an excitation energy E_a, the electron is promoted from the ground state to a higher vibrational state of the excited state. The position and width of the absorption band are determined by the central position of the ground state and the shape of the potential curve. The transition that occurs is "vertical" (based on Frank-Condon principle) because normally the electron transition is faster than the lattice relaxation.After absorption, the electron relaxes into the lowest level of the excited state $m = 0$ accompanied by emission of phonons and then returns into the ground state level (luminescent emission with energy E_e). The wavelength and width of the emission band is dependent on the potential curve of the excited state.
The displacement ΔR between the excitation and the relaxation process is the cause of line broadening, and if this effect is large we could have a non-radiative transition because the electron returns to the ground state via the

potential curve. The displacement is temperature dependent and becomes more important at higher temperature (this effect is known as "thermal quenching").

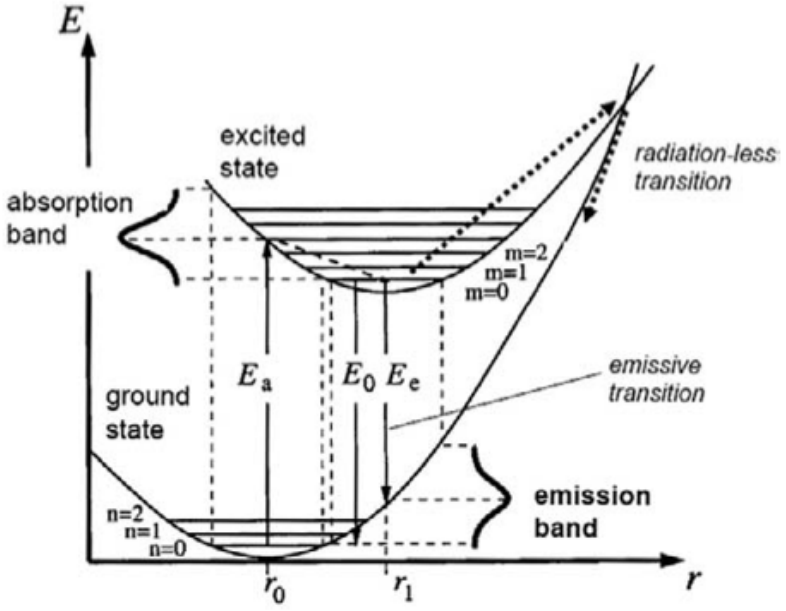

Figure 4.3: *Potential energy curves of the absorbing centre as a function of the relative distance R of the nucleus to the equilibrium position.*

4.3 Practical aspect of Cathodoluminescence spectroscopy

4.3.1 Interaction electron probe sample and generation of CL signal

When an electron beam strikes a solid surface, several processes occur. Normally the electron beam penetrates into the specimen and interact with the microstructure through the collision of the electrons with the atoms. Since the colliding particles are charged, the interaction are governed by electrostatic forces. Considering the interaction between an electron with the microstructure, two phenomena can arise: the electron hits an atomic nucleus, that hardly changes its position and is deflected without significant energy loss (elastic scattering) or the electron collides with the electrons of the atomic shells and part or all of the energy is transferred to the target electrons (inelastic scattering). Both scattering processes operate simultaneously and

provide a wide variety of useful signals such as emission of secondary electrons, back scattering electrons, Auger electrons, characteristic X-ray and cathodoluminescence emission, even if most of the electrons are absorbed (sample current) and converted into heat (phonons). As a consequence of these scattering processes, an electron probe spreads over a great volume after penetrating the specimen, as illustrated in figure 4.4. The shape and the size of this scattering volume depend upon the material, the beam energy and the angle of incidence of the electron beam.
However, not all the CL process arise from the excitation site, because energy transfer may occur due to the interaction with the lattice, and the site of emission can be distant [41].

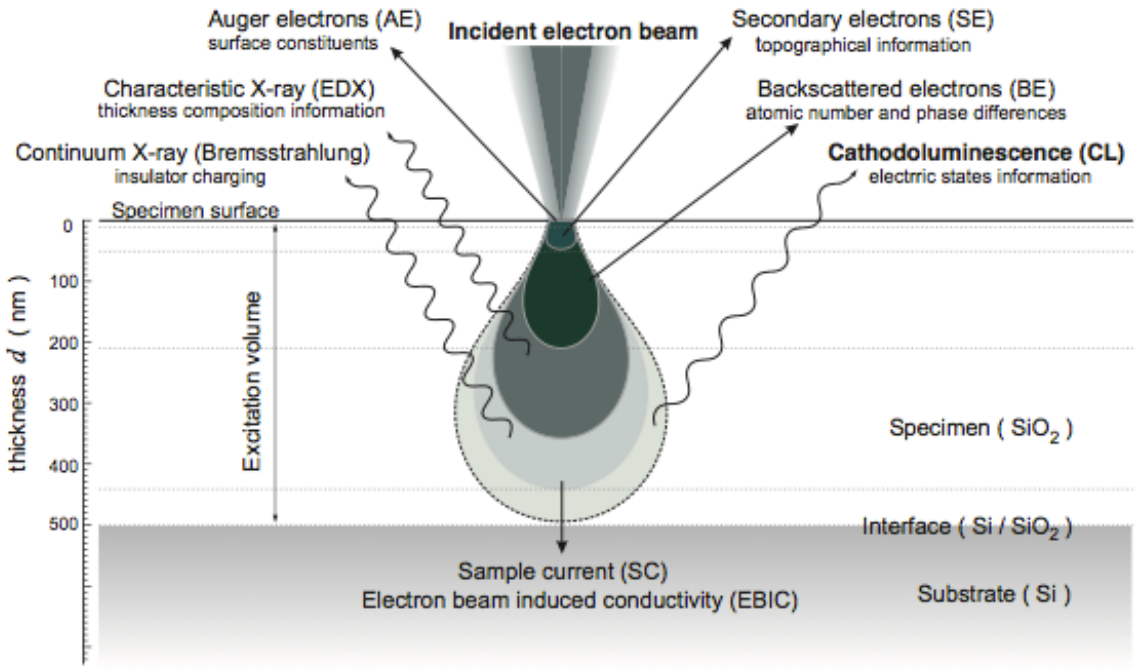

Figure 4.4: *Schematic representation of the processes resulting for electronic bombardment.*

To excite significant CL, in a semiconductor or insulator, the energy of electron beam must be limited otherwise the destruction of the specimen or of specific defects including luminescence centres could occur. For this reason, the

acceleration voltage used in CL measurement is rather low (1-10 keV). As a function of energy and intensity of the incident electron beam, to understand how the cathodoluminescence signal is generated, we should consider some aspect about the interaction between the electron and the matter. Indeed the dimension of the electron probe, determined of its energy, influence the penetration depth and the generation of electron-hole pairs, are fundamentals quantity in the determination the CL intensity.

4.3.2 Electron beam penetration range

As the result of different scattering events that the electrons undergo when penetrate into the solid, the original trajectories of them are randomised. An empirical expression for the range of electrons penetration as a function of the

$$R_e = \frac{k}{\rho} E_b^{\alpha} \tag{4.1}$$

energy of the electron beam E_b, was found by Everhart and Hoff [42]:
where ρ is the density of the material, k depends on the atomic number of the material and is also a function of energy; α depends on the atomic number and the electron beam energy E_b. A general expression for a wide range of atomic number and in agree with experimental results [43] was derived by Kanaya and Okayama [44]:

$$R_e = \left(\frac{0.0279 A}{\rho Z^{0.889}} \right) E_b^{1.67} \tag{4.2}$$

where E_b is in keV, A is the atomic weight in g/mol, ρ is the density in g/cm^3, and Z is the atomic number. Figure 4.5 shows a comparison of the electron generation range calculated according to the Everhart-Hoff and Kanaya-Okayama models for several semiconductors.

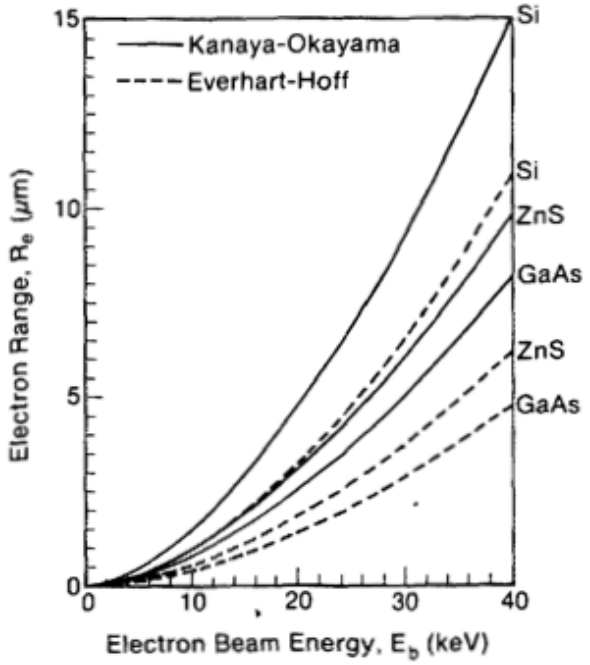

Fig 4.5: *Comparison of the electron beam penetration in function of its energy for different materials.*

4.3.3 Generation of electron-hole pairs

The shape of the excited volume depends both on the electron beam energy and the atomic number of the atoms which constitute the solids. For the same energy, the excited volume may be a drop shape for materials with low atomic number ($Z<15$), or spherical and semispherical shape for materials with respectively medium ($15<Z<40$) and high ($Z>40$) atomic number.
The shape of the electron probe is important because its determine the volume in which the electrons generate the electron-hole (e-h) pairs.
According to Yacobi and Holt [38], the generation factor, that is the number of the e-h pairs generated by an electron, is given by:

$$G = \frac{E_b(1-\gamma_e)}{\varepsilon_i} \tag{4.3}$$

where E_b is the electron-beam energy, ε_i is the ionization energy (i.e, the amount of energy needed for the formation of an electron-hole pair), and γ_e represents the fractional electron beam energy loss due to the backscattered electrons. This equation is of particular importance because ε_i has been found to be a constant for any given material, independent of the incident energy, and is related to the band gap energy E_g through:

$$\varepsilon_i = 3E_g \tag{4.4}$$

As a first approximation the *e-h* pair generation rate, within the electron probe volume can be calculated by the total electron energy loss profile [45], which can be expressed by the Bethe equation:

$$\frac{dE}{dS} = -2\pi e^4 N_A \frac{\rho Z}{EA} \ln\left(\frac{1.166E}{J}\right) \tag{4.5}$$

where E is the electron energy, S is the penetration depth and J is the average energy loss considering every possible events.
The CL generation rate in that volume, in materials that exhibit negligible minority carrier diffusion can be determined by integrating the total electron energy loss profile. Since the Everhart-Hoff equation (eq. 4.1) does not account for diffusion, it is not appropriate for modelling the spatial CL generation. Total energy loss profiles can be calculated accurately through Monte Carlo (MC) simulation of the primary electron in solid.

4.3.4 The CL intensity

Similarly with other spectroscopies the intensity of a CL emission band is the product of three terms expressing the generation of CL photons within the solid resulting from electron-atom interaction, the emission of CL photons resulting from generated photon-solid interactions and the experimental and instrumental parameters.

A general equation for the observed CL intensity, which is proportional to the number of *e-h* pairs created by the incident beam weighted by the radiative recombination coefficient η, is given by:

$$I_{CL} = F_D F_A F_R \eta \frac{G I_b}{e} \tag{4.6}$$

where F_D is a terms accounting instrumental factors, F_A is the absorption factor, and F_R is a factor accounting for internal reflection loss of CL intensity, η is the ratio of the radiative recombination rate to the total recombination rate and I_b the incident electron current. For insulating material in which CL is extrinsic in origin, is difficult obtain a unique expression for CL intensity as a function of the experimental conditions. The observed intensity is not only proportional to the *e-h* pairs generated; in fact during the irradiation the temperature increase, the bulk could change and the production of x-ray photons can modify the radiative and non-radiative transition probabilities. For these reasons the dependence between the CL intensity and the excitation is expressed by:

$$I_{CL} = f\left(I_b, d, t\right)\left(V - V_0\right)^q \tag{4.7}$$

where d is the beam diameter, t the irradiation time, V the electron beam voltage and q is comprised between 1 and 2 [46]

4.4 Instrumentation

The first application of CL spectroscopy, now outdated, has been made by using a fixed electron beam which irradiate the specimen surface.
The development of new scanning probe microscopy techniques has made possible the CL analysis by means of the scanning electron beam of SEM equipment, creating a coupled SEM-CL microscopy. Figure 4.6 show a schematic representation of a SEM-CL apparatus. SEM microscope can be equipped with optical devices that enable direct light collection from the specimen during the electronic bombardment. For this purpose, usually a

parabolic or ellipsoidal mirror are placed a short distance above the sample surface. The electron beam properly focused on the sample surface with electromagnetic lens, pass though an aperture on the mirror and impact the surface. The light generated from the sample, which is placed at the focus point of the mirror, is reflected to a detector. The mirror is not fixed and can be moved through a set of mechanical manipulators that allow the adjustment of the mirror position. The mirror reflects the light generated from the sample, placed on its focus point (see figure 4.7), into an optical fibre where is transmitted to a CCD detector that normally employ a PMT unit. The CCD allows the simultaneous collection of the entire range of wavelenght (from about 300 to about 800 nm) avoiding spectral distortions between the different λ-induced degradation of the sample during irradiation and by limiting the contribution of the background noise.

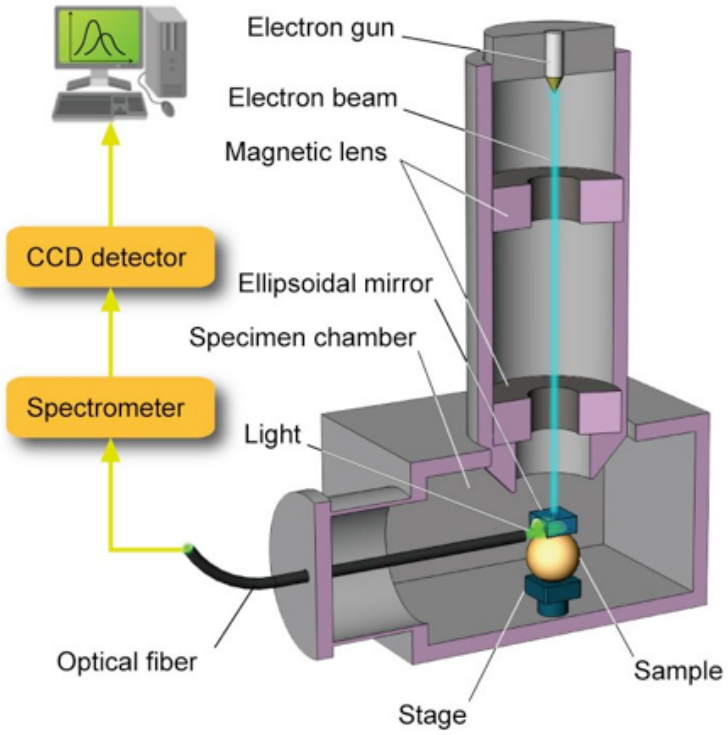

Figure 4.6: *Schematic representation of a coupled SEM-CL.*

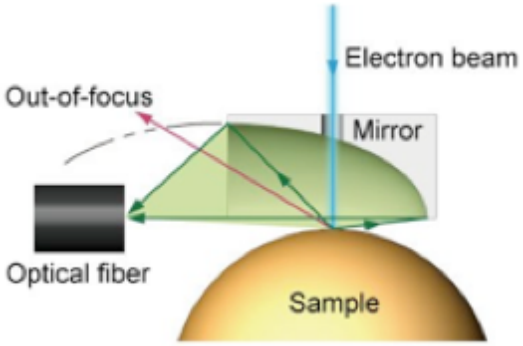

Figure 4.7: *Schematic representation of reflection by the mirror.*

4.4.1 Instrument used in this thesis

The cathodoluminescence measurements were performed by a field-emission scanning electron microscope (FE-SEM) with a Schottky-emission type gun (Hitachi S-4300 E) as the excitation source (Ceramic Physics Laboratory of Department of Materials Science and Engineering, Kyoto Institute of Technology). The FE-SEM was mounted on an optical table, which aiding the optical alignment and reducing the vibration. The specimen chamber is supplied by a "fast entry" system for the introduction and the extraction of the samples directly on the stage without changing in pressure. A high-sensitivity CL detector unit (Horiba MP-32FE) was employed for the collection of light upon reflection into an ellipsoidal mirror and transmission through an optical fibre. The spectrum of the emitted light was analyzed using a high-resolution monochromator (Horiba/Jobin Ivon-Spex TRIAX 320), equipped with a charge-coupled device (CCD) camera.

Chapter 5

Synthesis and characterisation of N:SiO_2 systems

In recent years, many deposition technique has been used to synthesize silicon oxynitride amorphous thin films, including chemical vapor deposition (CVD), laser ablation, vacuum evaporation, ion implantation and sputter deposition. [47-51]. The main drawbacks in CVD methods are that the deposited films is the may contain a significant amount of hydrogen incorporation due to the precursors used in that process. As consequence thermal treatments are necessary to remove the undesired hydroxyl groups.

The sputter deposition probably is the most suitable technique that allows a production of glass thin films at relatively low temperature with a small amount of contamination. In the literature, several investigations has been made for the CVD synthesis of both silica and silicon oxynitride films while only few research groups report the production of this system by the mean of sputter deposition. trough magnetron sputtering, different approach can be considered to produce silicon oxynitride films; with the usage of different target material, as well as different reactive gas in the chamber, it is possible to obtain different composition of the films. Generally, silicon target in a gas reactive mixture composed by N_2/O_2 is the most used approach to synthesize silicon oxynitride films. As reported by many research groups [52-55], different films stoichiometry could be obtained by changing the molar ratio between the component of the gas mixture. As a results silicon-rich

oxynitride, embedding silicon nanocluster, could be obtained. However, an alternative method to fabricate silicon oxynitride thin films, rarely reported in literature, is the use of SiO_2 target in nitrogen atmosphere [23]. With this approach, the silica is sputtered in its molecular form and can react with the nitrogen present in the chamber forming SiO_xN_y amorphous structure. Obviously, as stated in chapter 3, radiofrequency supply is needed to be able to sputter dielectric material. These methods of deposition have been chosen to prepare a-SiO_xN_y because the intent is fabricate stoichiometric compound in which the nitrogen is present only in small concentration as a dopant.

5.1 Synthesis of silicon dioxide and silicon oxynitride

5.1.1 Generalities of deposition

All depositions were performed in the Material Science Laboratory (in Mestre) by radio frequency (RF) magnetron sputtering, starting from silica target (SiO_2, 99,9999 % purity) in an atmosphere composed by Ar/N_2 gas mixture. The radiofrequency power is delivered by an RF generator (at 13.56 Hz) and magnetron source used was positioned to obtain the maximum rate configuration, which promote a homogeneous deposition on the substrate. In order to achieve higher uniformity deposition, the rotation of the sample holder was set at 5 rpm. The temperature of the sample holder during the depositions was maintained near to the room temperature (RT). The depositions have been made on high grade fused-silica slides (HSQ300, 25×75 mm^2, 1 mm thick). Before being used for the deposition, the silica slides were preliminary washed with soap and water and then were subjected to a four-step cleaning cycle in an ultrasonic bath with deionized water, trichloroethylene, acetone, and isopropyl alcohol in order to remove possible surface contaminations. To identify the slides a numbering was carried out through an incision with a diamond tip. Also, in order to perform measurements of the deposited thickness, some slides were masked in a corner before being placed in the sputtering chamber. All depositions were performed achieving the vacuum in the sputtering chamber by means of a cryogenic pump, in order to decrease the amount of OH^-. Immediately before the deposition a 20 minutes pre-sputtering

stage (RF-biased) was performed both on substrate as well on target material to chemically activate it.

5.1.2 Synthesis

Preliminary study conducted by Cattaruzza et al. [56, 57] report that pure Ar atmosphere, at pressure of 50×10^{-4} mbar and SiO_2 power source of 250 W are the best conditions to deposit amorphous silica thin film with a deposition rate approximately of 700 nm per hour. In order to incorporate a low amount of nitrogen in the structure, a gas mixture of Ar/N_2 was used. By changing the relative partial pressure of the gaseous phase, maintaining the total pressure at 50×10^{-4} mbar, it was possible obtains silicon oxynitride films with various nitrogen content. The films were deposited without intentional heating (i.e. RT).

Three silica slides were used as a substrate for each deposition. The different argon and nitrogen partial pressure, the deposition time and the measured thickness of the synthesize silica and silicon oxynitride thin films are presented in table II. Since Ar is more efficient target bombarding gas than nitrogen, as the Ar/N_2 ratio decrease the sputtering rate also decrease. Indeed the sputtering time was varied to achieve to obtain comparable thickness in the deposited films.

Sample N°	P (Ar) (mbar)	P (N_2) (mbar)	Thickness (μm)	Dep. time (hours)
SiO_2	50×10^{-4}	/	1.70 ± 0.05	2
SiO_2-N (5)	45×10^{-4}	5×10^{-4}	0.82 ± 0.02	2
SiO_2-N (10)	40×10^{-4}	10×10^{-4}	0.72 ± 0.02	2
SiO_2-N (15)	35×10^{-4}	15×10^{-4}	1.00 ± 0.2	3
SiO_2-N (20)	30×10^{-4}	20×10^{-4}	0.95 ± 0.3	3
SiO_2-N (25)	25×10^{-4}	25×10^{-4}	1.10 ± 0.05	3.5

Table II: *Sputtering conditions and films thickness for SiO_2 and SiO_2-N.*

In order to perform annealing treatments of the as-deposited samples, each silica slides were cut by the mean of a diamond tip into ten pieces, 12.5×15 mm^2 of size. Each of these samples was annealed at a different temperature from 50°C up to 1200°C, for one hour in air. The annealing treatments were performed by a "heating apparatus" which can achieve temperature up to 1400°C. The samples were introduced into the heating chamber inside a metallic crucible in order to uniform the heat propagations.

5.2 RBS analysis

To check the local stoichiometry of the system as well as the presence of nitrogen in the matrix, an RBS analysis were performed on the as deposited samples for both pure SiO_2 and SiO_2-N (25). RBS spectra obtained is shown in figure 5.1, 5.2.
Since the nitrogen amount is below the RBS detection limits, its concentration was determined by a comparison of the two spectra, considering that the lacking oxygen is bonded with nitrogen present in the structure.

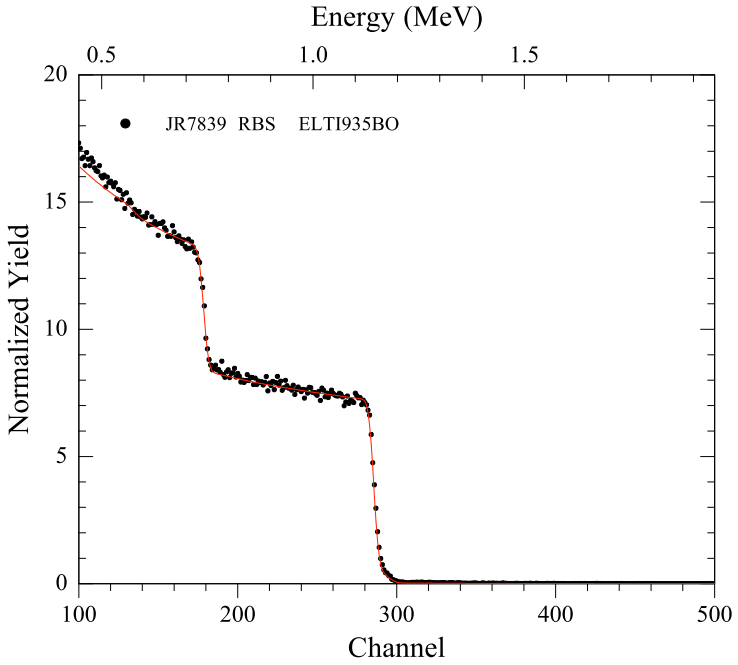

Figure 5.1: *RBS spectrum of SiO_2 RT*

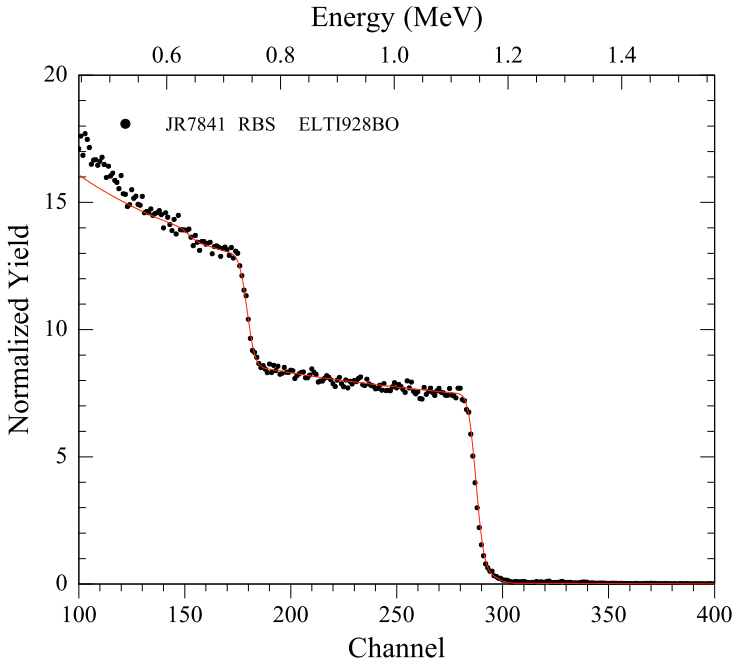

Figure 5.2: *RBS spectrum of SiO_2-N (25) RT*

Films stoichiometry, nitrogen concentration, and dose are reported in table III. From RBS analysis is also possible estimate the films thickness, starting from the density of bulk silica, assumed 2.2 g/cm^3. The results obtained are slightly lower than the thickness measured with the profilometer: this indicates that the density of our deposited silica is lower than the bulk one. It is possible to notice that, in the pure silica, the estimated molar ratio between Si and O is a bit over-stoichiometric. The nitrogen concentration reported correspond to an atomic percentage of 7%, result in agreement with the XPS analysis reported in subsection 6.2.

Film Stoichiometry	N dose (atoms/cm^2)	N conc. (atoms/cm^3)	Thickness estimated (μm)
$Si_1O_{2.1}$	/	/	1.45
$Si_1O_{1.8}N_{0.2}$	4.8×10^{17}	6×10^{21}	0.79

Table III: *RBS analysis results for SiO_2 and SiO_2-N.*

5.3 Thin films morphology and post deposition annealing effect

Thin films microstructure of the deposited film typically depends on the gas pressure in the deposition chamber as well as the ratio between the substrate temperature and the melting point of target material. Since the total pressure and the substrate temperature were the same in every deposition, all the as-deposited films present a similar morphology.

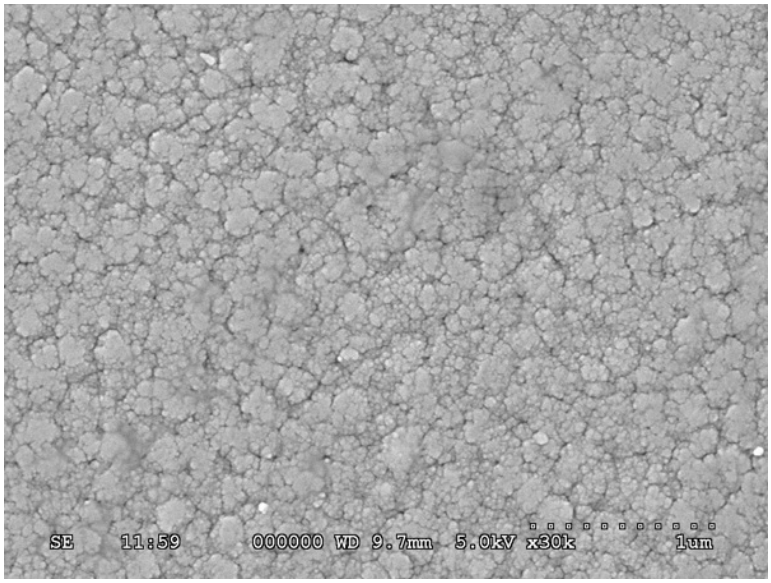

Figure 5.3: *SEM micrograph of SiO_2 RT*

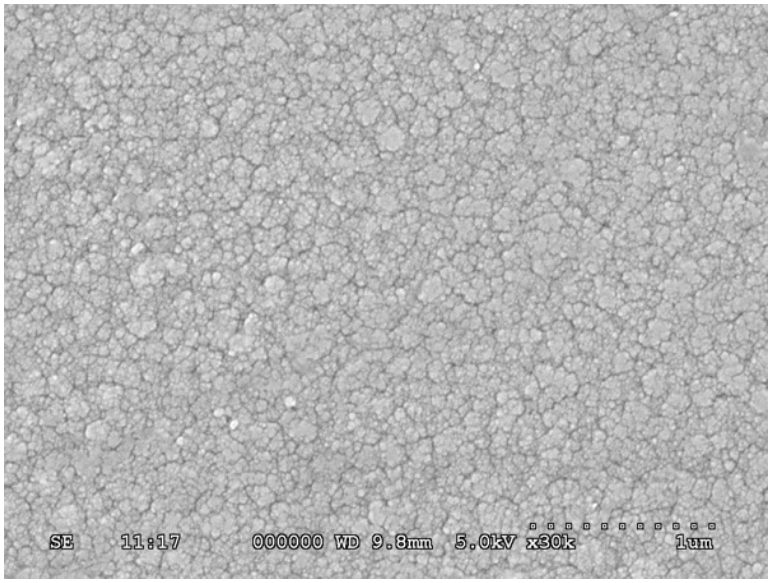

Figure 5.4: *SEM micrograph of SiO_2-N (25) RT*

Figure 5.3 and 5.4 present the SEM micrographs for SiO_2 and SiO_2-N (25) as-deposited samples. As shown, the film formed consist in a randomly granular structure. As reported by Thornton in his review [59] the thin films structure deposited by magnetron sputtering can be divided in several kind, which depend on the various deposition parameters. The two mains controlling factor are: the ratio of substrate temperature to the melting temperature (of the thin film material) and the working gas pressure. As suggested by the author, using a high pressure of working gas and a low ratio between the substrate temperature and the material melting point a structure consisting of "tapered crystallites separated by voids" is expected. As the working gas pressure is decreased, less scattering occurs and the arrival energy of the sputtered material increases. The film formed in this condition, still presents a granular structure but more compact. As a matter of fact, the SiO_2 morphology presents some voids in comparison with the SiO_2-N (25) this could be due to the different effect of the pressure of the two working gas used (Ar and Ar/N_2): for instance, the film synthesized in mixed Ar/N_2 grows slowly improving its microstructure homogeneity.

In general post-deposition annealing can have dramatically impact on the film microstructure as well on its adhesion with the substrate. If the substrate material has a different linear expansion coefficient than the sputtered films, during the thermal treatments interfacial stresses can be accumulated leading even to fracturing the material. In this study, all the deposition were made on silica slices in order to have the best matching between the deposited material and the substrate. Indeed annealed samples shows good adhesion with the substrate even at the highest temperature. SEM micrographs show that the surface morphology of all the annealed samples (both pure silica and silicon oxynitride) remains unaltered up to 1100°C annealing temperature, above which the structure begin to exhibit a matrix densification. As reported in literature [60], it is estimated that the amorphous silica glass transitions temperature (T_g) is comprised between 1000-1300°C. However, a difference is noticed with the comparison between SiO_2 and SiO_2-N (25), in which the "glassy state" is more evident. It seems the nitrogen content decrease T_g, but

no literature data has been found, and no accurate measurement has been taken on this system.

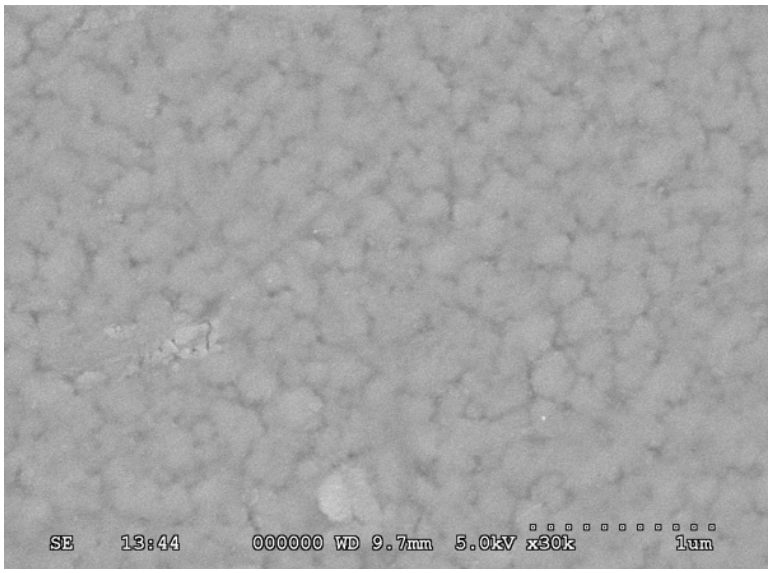

Figure 5.5: *SEM micrograph of SiO_2 annealed at 1200°C*

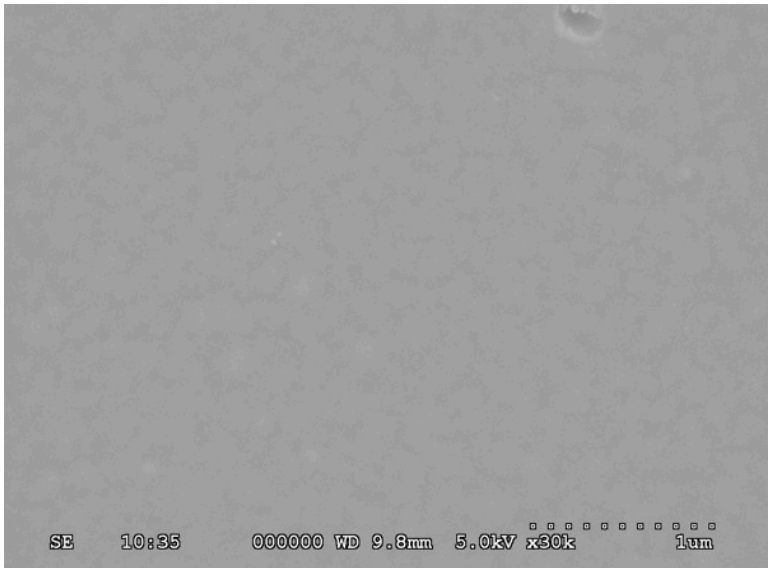

Figure 5.6: *SEM micrograph of SiO_2-N (25) annealed at 1200°C*

Chapter 6

Spectroscopical results

6.1 Cathodoluminescence characterization

6.1.1 Experimental conditions

Before being introduced into the specimen chamber, the samples were fixed with C-tape and dotie on an aluminium plate; to avoid charging, induced by the electron beam, a 7 nm-thick layer of platinum was deposited on their surface. All CL spectra were recorded with the same experimental condition. The electron beam acceleration voltage was kept at 5 KeV with a probe current of 180 pA (for 10 s of irradiation). Low acceleration voltage was chosen to prevent both the temperature related wavelength shifts, that could arise from elongated electron irradiation time, and to not expose the structure to beam damage. Working distance calibrations, which affects the intensity of the spectrum collected, has been made respect to a GaN standard reference signal. Indeed to check the electron beam efficiency and in order to obtain an independent spectral calibration of the spectrometer a CL spectrum from GaN and the signal from a mercury-neon discharge lamp, was collected every three measured spectra, respectively. From each sample several spectrums were collected in order to check if the sample present local composition different than other point. Data treatments of obtained spectra were realized with the data analysis software Origin Pro 8.5.1.

6.2 SiO_2 cathodoluminescence

CL spectrum collected for un-doped SiO_2 and its relative deconvolutions is shown in figure 6.1.

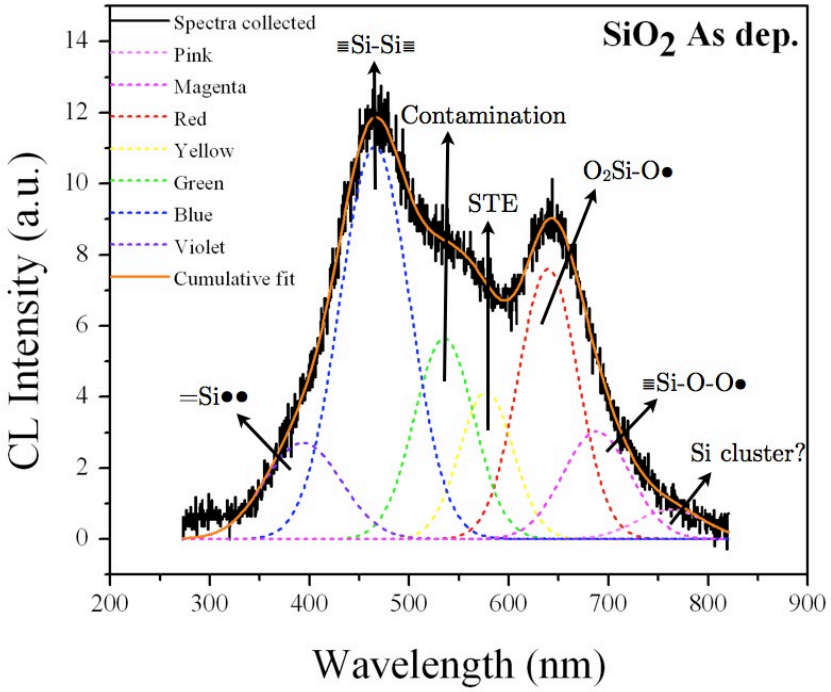

Figure 6.1: *CL spectra and relative deconvolution of SiO_2 as deposited.*

Normally, CL spectrum of SiO_2 is composed by several overlapping band, which can be found performing a suitable fitting procedure of the spectrum obtained. According to the literature [60], the fitting procedure selected is based on a spectral deconvolution involving 7 gaussian sub-bands, whose positions were superimposed in correspondence with the local maximum intensity in the spectra. The spectral deconvolution shows that the CL spectrum of silica consists of seven overlapping band. All these bands, already reported in the literature, are originated by a mechanism of defects induced luminescence center. Table IV report the attribution of the deconvoluted gaussian bands, according with L.Skujia [61] and R. Salh [62].

Band (eV)	λ_c *(nm)*	*Description*
Violet (3.1)	394 ± 3	Twofold coordinated silicon (ODC(II)) =Si••
Blue (2.64)	468 ± 3	Neutral Oxygen Vacancy (ODC(I)) ≡Si-Si≡
Green (2.32)	534 ± 4	Contamination Band
Yellow (2.15)	576 ± 4	Self Trapped Exciton (STE)
Red (1.93)	639 ± 2	Non Bridging Oxygen Hole Center (NBHOC) O_2Si-O•
Magenta (1.8)	687 ± 2	Peroxyl Radical Center (POR) (?) ≡Si-O-O•
Pink (1.62)	763 ± 3	Silicon nanocluster/ Interstitial O_2 (?)

Table IV: *Summary of the luminescence band in a-SiO_2.*

The bands obtained from the deconvolution are supported by literature, in which a lot of defect types have been discussed, and many reproduction models have been proposed for each one. Many aspects regarding the nature of the defects associated bands and are still controversial and not yet completely understood, especially for the near-IR region. Defects present in silica are related to locally oxygen deficiency or oxygen excess in matrix. Bands present in blue (394, 468 nm) and red (639, 687 nm) region are respectively associated to the presence of oxygen deficiency centers and non bridging oxygen hole centers. Another band in the green region, arise from the presence of a carbon contamination or structural water, around 530 nm. The accumulation of contamination during low voltage measurement in the vacuum environment is an intrinsic problem of conventional SEM apparatus [43]. Further luminescence band of relative intensity can be found in the yellow region around 576 nm, which has been ascribed to a self trapped exciton. For the near-IR the assignment of the band is still unclear. The band at 763 nm can be either related to the presence of interstitial molecular oxygen or to silicon aggregate

and their presence could depend on the local silica stoichiometry. Also, it possible consider this band as a spectral artefact due to the broadening of the closest peak.

In the next subsections, an explanation on the origin and formation of both oxygen deficiency or excess related defects in silica is reported.

6.2.1 Oxygen-deficiency related defect (3.1 - 2.7 eV)

The main family of optical active diamagnetic defects in silica are the oxygen-deficiency centers (ODC), which luminescence are found in the blue region of the spectra between 350 and 460 nm. The band found at 468 nm (≈2.7 eV) can be labelled as ODC(I) [63]. This defect center is characterized simply by a neutral oxygen vacancy and indicated generally as ≡Si—Si≡. However, this configuration, identifies just one of possible structure associated to oxygen related defect. As reported in literature by Skujia et al. [64] the ODC could be described by another different possible model: the twofold coordinated silicon ODC(II), denoted as =Si••, with two unpaired electrons lying on the silicon atom. Nishikawa [65] and other authors [66] concluded that the band founded at 394 nm (3.1 eV) arise from this kind of defects. Figure 6.2 shows a schematic illustration of the transformation from a neutral oxygen vacancy to a twofold coordinated silicon.

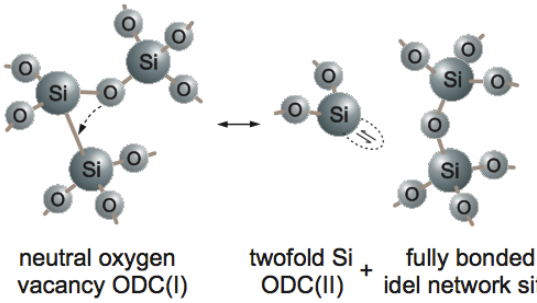

Figure 6.2: *Possible ODC(I) to twofold Si ODC (II) transformation.*

The assignment of ODC(I) to an oxygen vacancy is universally accepted, but on the contrary many controversial over the basic structure of ODC(II) and its formation are stated in literature. Another hypothesis for ODC (II) have been suggested by Imai et al. [67] which represent the ODC(II) as an unrelaxed oxygen vacancy, denoted as ≡Si···Si≡. Figure 6.3 shows a schematic illustration of the transformation between the ODC(I) and the "unrelaxed" ODC(II).

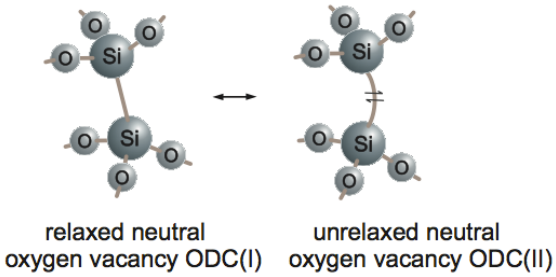

Figure 6.3: *Possible ODC(I) → unrelaxed ODC (II) transformation.*

The mechanism of the luminescence generated by both relaxed and unrelaxed neutral oxygen vacancy have just recently found an explanation. First observation conducted by Imai et al. report that an 7.6 eV absorption band in irradiated as grown a-SiO_2 could be ascribed to the neutral oxygen vacancy ODC(I). In addition, two bands at 4.4 eV and 2.7 eV have been observed during irradiation at 5 eV, 6.9 eV or 7.6 eV [61]. The 4.4 band that was previously associated to oxygen relate defects by Jones et al. [68], can be ascribed to the ODC(II), while the 2.7 eV band can be associated to the ODC(I). This transition were also confirmed thought a computational approach by Pacchioni et al. [69]. The calculations support the assignment of the 7.6 eV band to a $S_0 \rightarrow S'_1$ transition in a neutral oxygen vacancy. The first allowed radiative transition is corresponds to the formation of two unpaired electrons, coupled singlet, on the adjacent silicon atom.
Considering their lifetimes, the 4.4 eV and 2.7 eV bands have been ascribed to singlet-singlet ($S_1 \rightarrow S_o$) and triplet-singlet ($T_1 \rightarrow S_o$) transitions at the site of oxygen-deficient type defects, respectively.
Nishikawa et al. [70] study the decay kinetic of the 4.4 eV band, reporting a diagram of the energy level for the optical transition, as reported in figure 6.4

where the non-radiative mechanism of relaxation are represented by the dotted arrow.

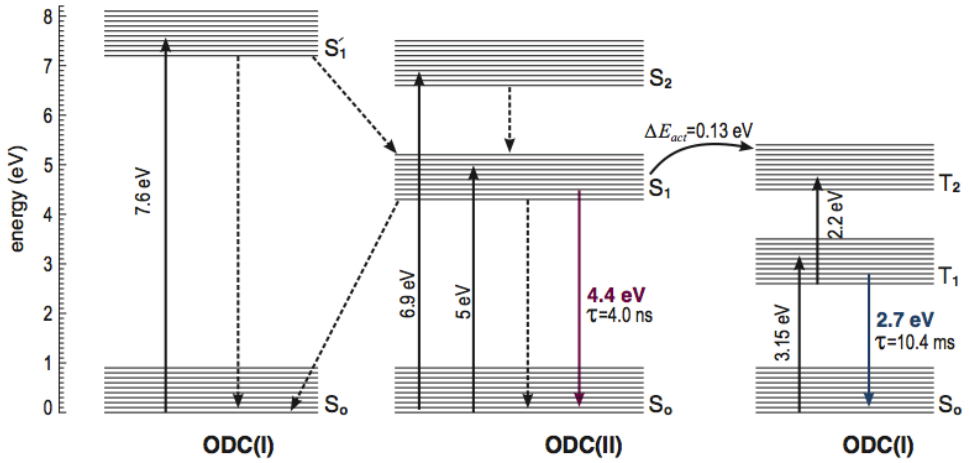

Figure 6.4: *Energy diagram of ODC(I) → ODC (II) transformation.*

However, Nishikawa report that in a particular type of high-purity silica, during 5 and 7.9 eV irradiation, a 3.1 eV band is observed. The decay constant is relatively slow if compared with other luminescence bands which have shorter lifetimes, such as the 4.4 eV band, with a lower decay constant. Since the 4.4 and 3.1 has the same absorption band, is reasonable to think that they represent different state of the same ODC(II) defect. The author conclude that the 3.1 eV band, which is evident in the present work, is associated to the twofold coordinated center.

It should be notice that ODCs are not the only oxygen related vacancies in the silica structure. Another family of defects are represented by the E'-centers, associated with the 5.85 absorption band, which consist in a dangling tetrahedral orbital of a silicon atom, bonded with three oxygen, and an unpaired electron (fig 6.5). This center also denoted as ≡Si• are usually characterized by means of EPR spectroscopy, while cannot be detected with cathodoluminescence because does not possess a radiative decay mechanism [71].

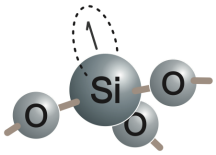

Figure 6.5: *E' center.*

6.2.2 Oxygen excess related defects (1.93 - 1.8 eV)

The absorption band in the red part of the visible light spectral range, around 640 nm is associated to one of the most characteristic defect in silica glass, the non-bridging oxygen hole center (NBOHC). This defect represents the simplest elementary oxygen-related intrinsic defect in silica and can be considered as the product of the breaking bond between silicon and oxygen in the silica basic unit, which resulting in the NBOHC and E' centers, as showed schematically in figure 6.6.

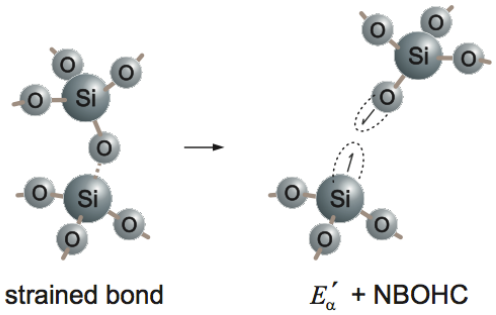

Figure 4.6: *E' and non bridging oxygen hole center (NBOHC)*

Some authors have suggested different mechanism for the formation of NBOHC resulting in an energy variation of the spectroscopic transition responsible for the absorption in the red region. One of this possible mechanism was proposed by Munekuni et al. [72] which states that NBHOC can be originate from the rupture of a peroxy linkage, which can be found in oxygen-excess silica:

$$\equiv\text{Si-O-O-Si}\equiv + e^- \rightarrow \equiv\text{Si-O}\uparrow \ ^-\text{O-Si}\equiv \tag{6.1}$$

As confirmed by computational calculation [69] the fragment $^{-}$O-Si$\equiv$ which present an absorption band around 4.8 is another possible candidate for the luminescence in the red region.

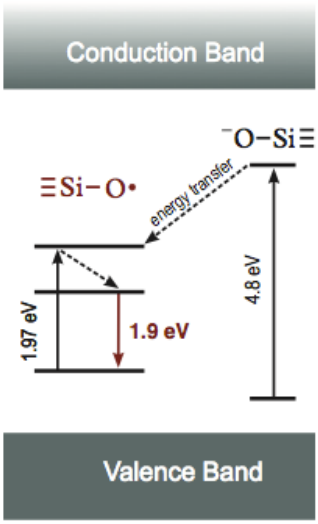

Figure 6.7: *Energy transition for NBOHC.*

Peroxy linkage could be involved in the creation of another defect related to the oxygen excess: the peroxy radical (POR). Other channels are also possible for the creation of POR such the reaction of interstitial oxygen with silicon dangling bond, as well the reaction of atomic oxygen with a NBOHC.
This defect is paramagnetic, with a hole delocalized over anti-bonding π-type orbitals of the O—O bond in the structure (fig 6.8).

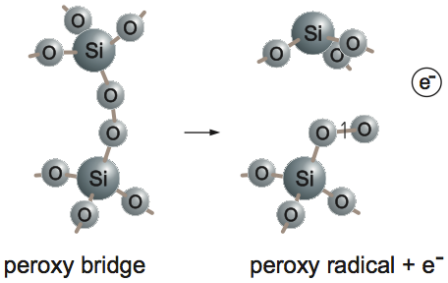

Figure 6.8: *Peroxide radical (POR).*

However, the optical properties of POR in silica are unclear, with some disagreements on the value of its energetic transition. Some authors report the absorption band of POR located in the red range [61,62] between 1.8 and 2 eV, but lower than the NBOHC position. The luminescence band found at 687 nm in the CL silica spectrum can be assigned to this type of defect.

6.2.3 Self trapped exciton (STE)

The band founded in the yellow-green region, at 575 nm can be ascribed to a self trapped exciton. The existence of the self-trapped excitons in amorphous SiO_2 is supported by experimental measurements, extensively investigated by Fitting et al. [73]. The self-trapping is due to the displacement of an oxygen atom from a regular lattice site into an interstitial site, with the formation of an E' center at one of the silicon near the vacancy. As a consequence of the displacement, a hole is localized onto that oxygen, while an electron is self-trapped onto one of the two neighbour atoms, forming a threefold coordinated silicon (Fig 6.9). The STE absorption energy is explained at 5.2 eV and is due to the electronic excitation component of the exciton coupled with an electron-phonon interaction. De-excitation of this defect gives rise to a radiative emission around 2.1 eV [74].

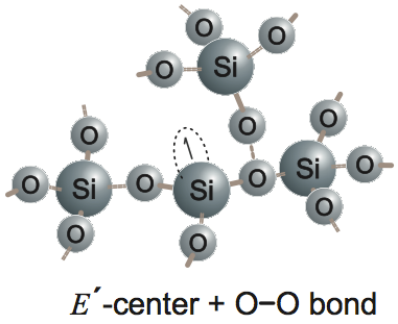

Figure 6.9: *Self trapped exciton (STE).*

6.3 Thermal Annealing

CL spectra collected from as deposited and 200, 500, 750, 1000, 1200°C annealed SiO_2 samples are showed in figure 6.10. Spectra reported, collected at intermediate temperature, are the most representative of the un-doped annealed silica.

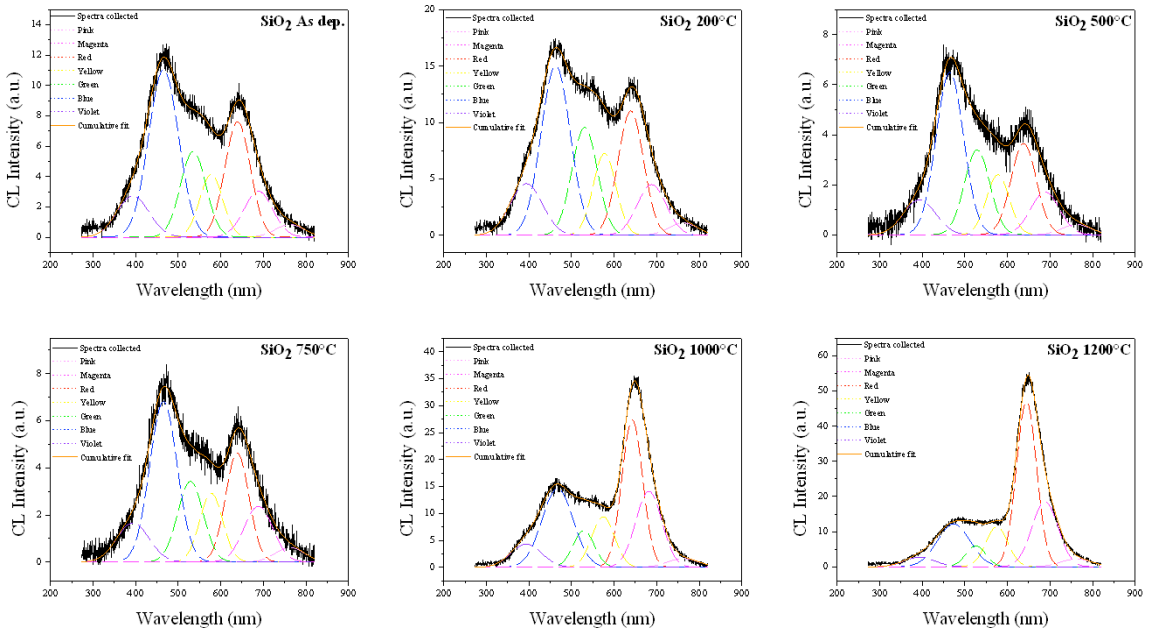

Figure 6.10: *CL spectra collected for as dep. and 200, 500, 750, 1000, 1200°C annealed SiO_2 .*

CL spectra, present two evident peaks at 460 and 640 nm, respectively, a low wavelength shoulder that is evident only in as deposited, 200 and 1000°C annealed sample, and a mild peak, located at 550 nm. Spectra was deconvoluted with the same 7 gaussian curves discussed in the previous section, which are located at the same energy position showing the same FWMH. The annealing treatments influence the defects population in the silica matrix, modifying the relative intensity of the associated luminescence bands. From the collected spectra, it is clear that the behaviour of the oxygen excess defects dramatically increases after at 1000°C, giving rise to a strong luminescence emission.

However, the oxygen-deficiency relate, the yellow and the green bands show a lower alteration than the red band.

Figure 6.11 show the maximum intensity of the main deconvoluted band in as a function of the annealing temperature. To compare the results obtained from the deconvolution a general trend of such bands is obtained through a polynomial interpolation of the collected data.

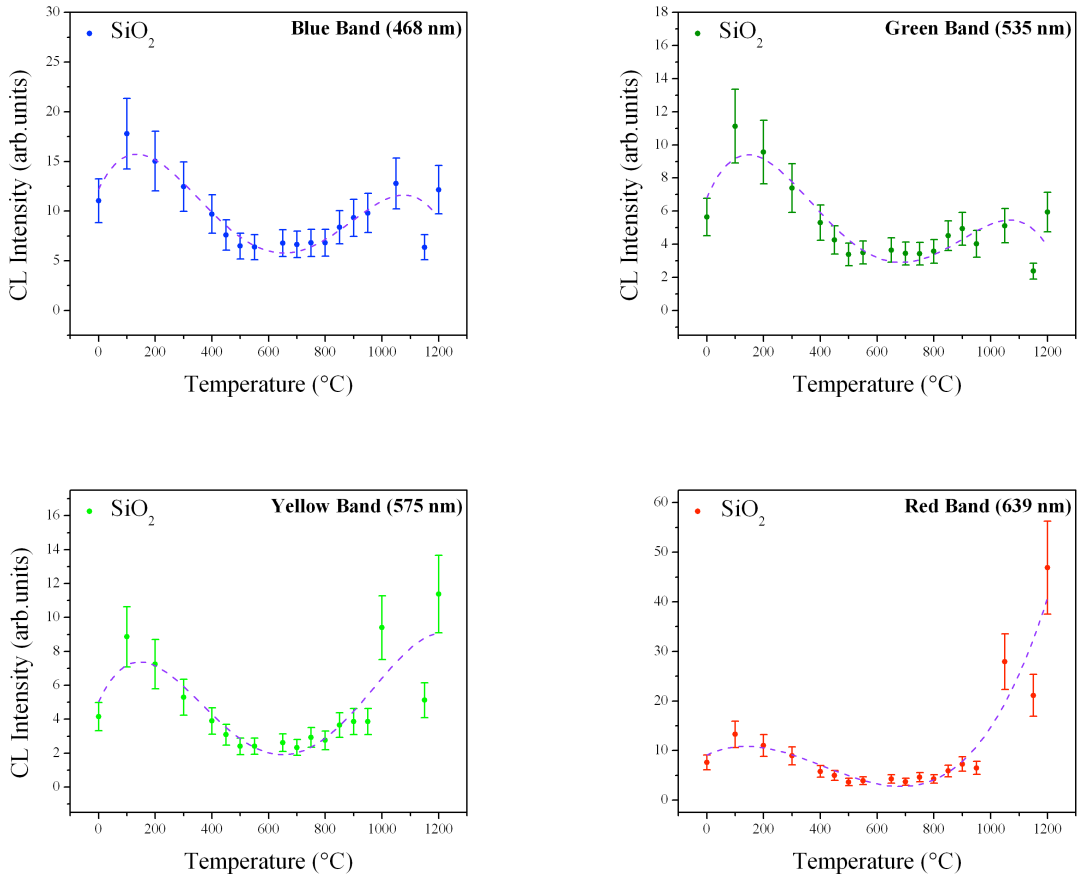

Figure 6.11: *Maximum intensity of blue, green, yellow and red bands in function of temperature.*

In the first part of temperature range, is possible to notice a progressive decreasing of each defect-associated bands. For annealing temperature lower than 600°C, the thermal treatments of RT synthesized silica films seems to quench the luminescence generated from defects. Since the CL intensity is

related to the generation factor of *e-h* pairs (eq. 4.6) which depends upon the population of a specific defect, in the first instance this decrease of luminescence can correspond to the decreasing of the defect popultion.
An explanation of this behaviour has been given by Brückner in his studies of silica glass [75]. Brückner suggested that the relaxation process, due to the relaxation of internal structural stresses in this temperature range, is partly connected with a healing process for "open bonds" and that during the first heating up chance occasional linking of Si-O bonds occurs. For this reasons, NBOHC and POR oxygen-excess relate bands and STE band, related to a threefold coordinated silicon surrounded by an O-O bond, decrease. The decreasing of the ODCs band, when silica is annealed at 500°C in oxidant atmosphere was also noticed by Jones et al. [68], which propose that oxygen fills the vacancy center.
The yellow luminescence band, ascribed to the presence of contamination such structural water [76] or carbon contamination at the surface [60], decrease because the thermal treatment can eliminate part of this contamination.

By increasing the annealing temperature towards 1000°C, CL spectra, especially in the red region exhibit important modifications. NBOHC band rapidly increase overcoming the intensity of the ODC band which does not undergo to such high modification. Contrary on the fist range of temperature the strong increasing of the red band indicate an increase of Si-O bond breaking in basic silica units. As a consequence, a threefold coordinated center and a NBOHC are originated from this effect (6.2). As s side effect, the two threefold silicon can reacts to form a Si-Si homobond creating an ODC center (6.3), or reacts with oxygen molecules of the atmosphere producing a POR (6.4). Indeed above 800°C a small increase in intensity is observed for the blue band.

$$\equiv\text{Si-O-Si}\equiv \rightarrow \equiv\text{Si}\bullet + \bullet\text{O-Si}\equiv \tag{6.2}$$

$$\equiv\text{Si}\bullet + \text{O}_2 \rightarrow \equiv\text{Si-O-O}\bullet \tag{6.3}$$

$$\equiv\text{Si}\bullet + \bullet\text{Si}\equiv \rightarrow \equiv\text{Si-Si}\equiv \tag{6.4}$$

Figure 6.11 show the comparison of the intensity trend of each deconvoluted bands. The violet band associated to twofold coordianated silicon and the near-IR band assigned to the presence of interstitial oxygen does not show any significant variation increasing the annealing temperature.

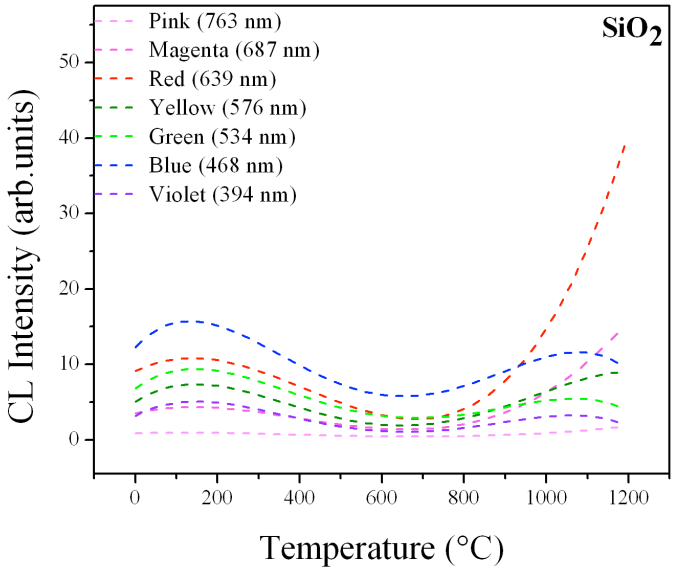

Figure 6.11: *Maximum intensity trend of each SiO_2 bands in function of annealing temperature.*

Some authors noticed that in artificial silica glass, annealed in the temperature range from 800°C to 1100°C, shows a volume dilatation [59, 74]. Of course, this is associated with the incoming glass transition temperature, which is found around 1150°C in this glass. However, since the samples annealed at high temperature above 700°C are subjected to slow cooling is expected that a reorganization of the network, in which the isolated Si and O atoms could link. On the contrary, the structural reorganization observed produce a high degree of "disorder". The hypothesis is that if a sample is annealed from temperatures above the glass transition temperature, a permanent defects distribution is built up which tends to a "metastable equilibrium" producing a "irreversible" or "permanent" changes of glasses chemical state with a characteristic set of luminescence bands.

This feature has been proved: the sample annealed at 1200°C, which probably reach the glass transition temperature shows a CL spectra very similar to those collected for commercial high purity fused-silica (HSQ300) annealed at 1200°C or room temperature. Figure 6.13 show the comparison between the spectra obtained form 1200°C annealed silica and from HSQ 300 fused-silica slide.

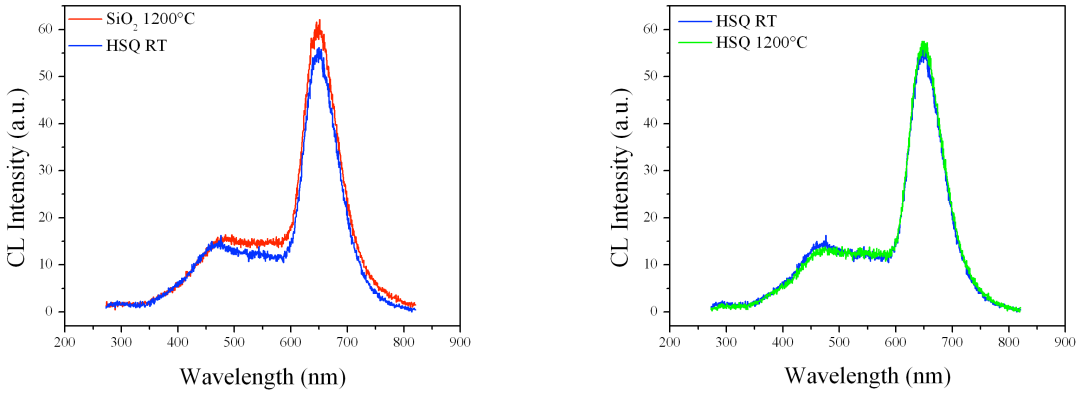

Figure 6.12: *Comparison of CL spectra collected from SiO_2 1200°C, HSQ (300) RT and 1200°C annealed.*

During the manufacturing process, the commercial silica reach processing temperature higher than 1200°C but present the same CL spectra of RT synthesise film through magnetron sputtering deposition. Also other authors that reports a CL investigation of defect centers in annealed a-SiO_2, [77] found the same characteristic sets of CL bands. It is possible suppose that this behaviour is independent of measurement condition and preparation procedure. In this studies for the first time the evolution of the CL bands from RT to the glass transition temperature is reported. CL spectra of low temperature annealing were never studied, because usually the temperature reached during preparation of the material is higher than the glass transition temperature. The results indicate that RT synthesized silica thin film annealed up to 600°C presented a lower defect population in comparison with higher annealing temperature.

6.4 Effect of N-doping

CL spectra obtained from as-deposited, and 200, 500, 750, 1000, 1200°C annealing temperature of N-doped SiO_2 at different nitrogen concentration are reported from figure 6.13 to 6.16. Spectra were collected with the same experimental condition of the previous CL analysis.

Without consider the deconvolutions, two consideration arise from the reported analysis: first, nitrogen doping even if in very low amount, modifies the defects luminesce emissions; this modification depend upon the nitrogen amount. Second, the general trend of the luminescence intensity with the annealing temperature present the same features of the un-doped silica glass.

As stated in chapter 2, during the deposition nitrogen gas can react with silicon or oxygen forming oxynitride of unknown stoichiometry (i.e. SiO_xN_y)

However, no additional luminescence bands grow-up when silicon oxynitride is formed, just a variation of the intensity of the pre-existing band in silica are measured.

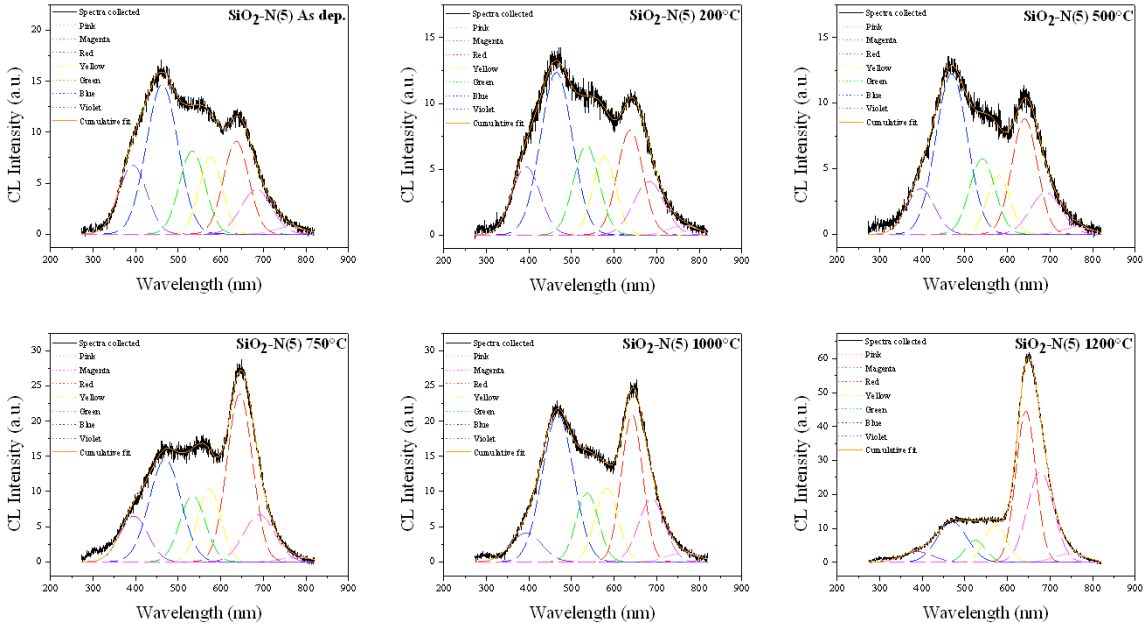

Figure 6.13 *CL spectra collected for as dep. and 200, 500, 750, 1000, 1200°C annealed SiO_2-N (5).*

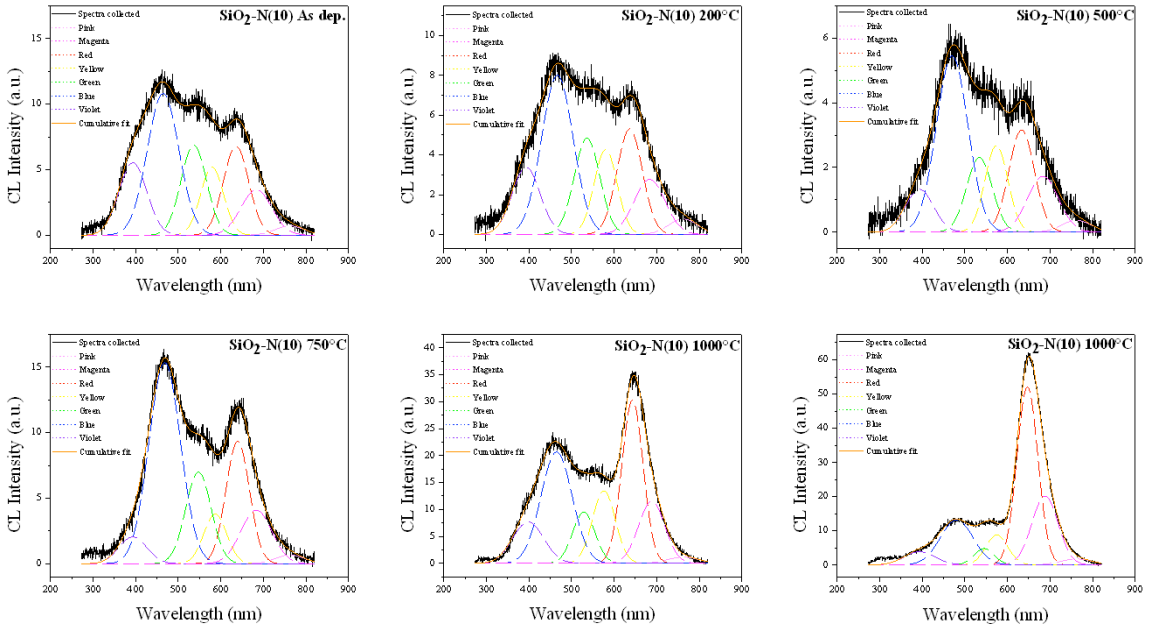

Figure 6.14 *CL spectra collected for as dep. and 200, 500, 750, 1000, 1200°C annealed SiO_2-N (10).*

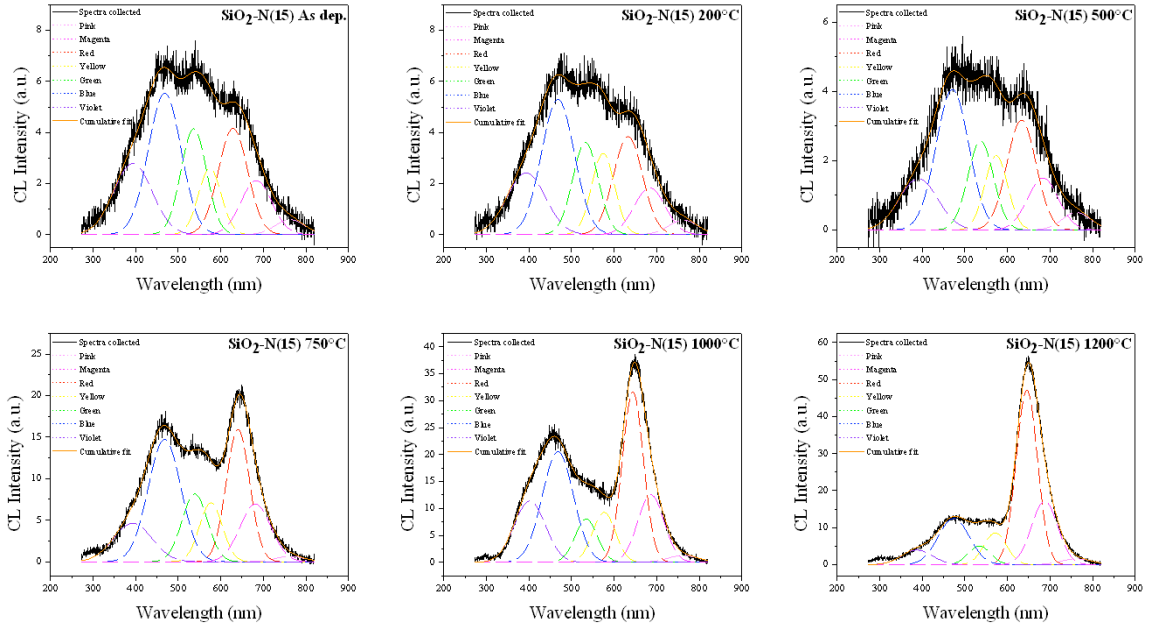

Figure 6.15 *CL spectra collected for as dep. and 200, 500, 750, 1000, 1200°C annealed SiO_2-N (15).*

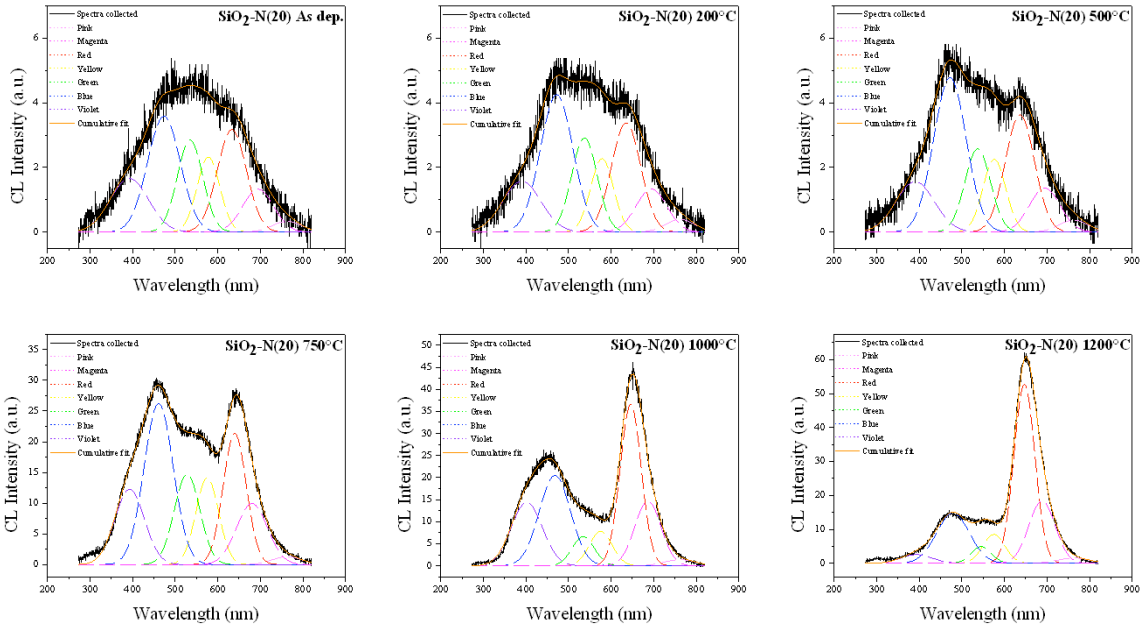

Figure 6.16 *CL spectra collected for as dep. and 200, 500, 750, 1000, 1200°C annealed SiO_2-N* (20).

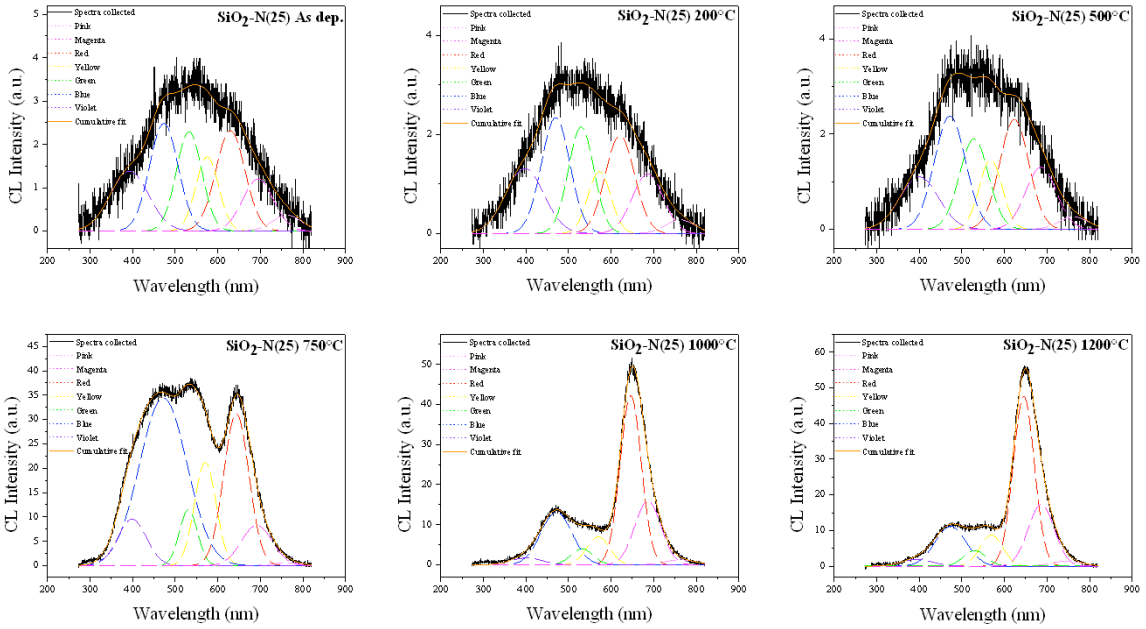

Figure 6.16 *CL spectra collected for as dep. and 200, 500, 750, 1000, 1200°C annealed SiO_2-N* (25).

The maximum intensity trend of the defects-related luminescence bands in function of the annealing temperature are reported in figure 6.19. By this representation it is evident how the progressive content of nitrogen introduced in the system modifies the mentioned CL bands.

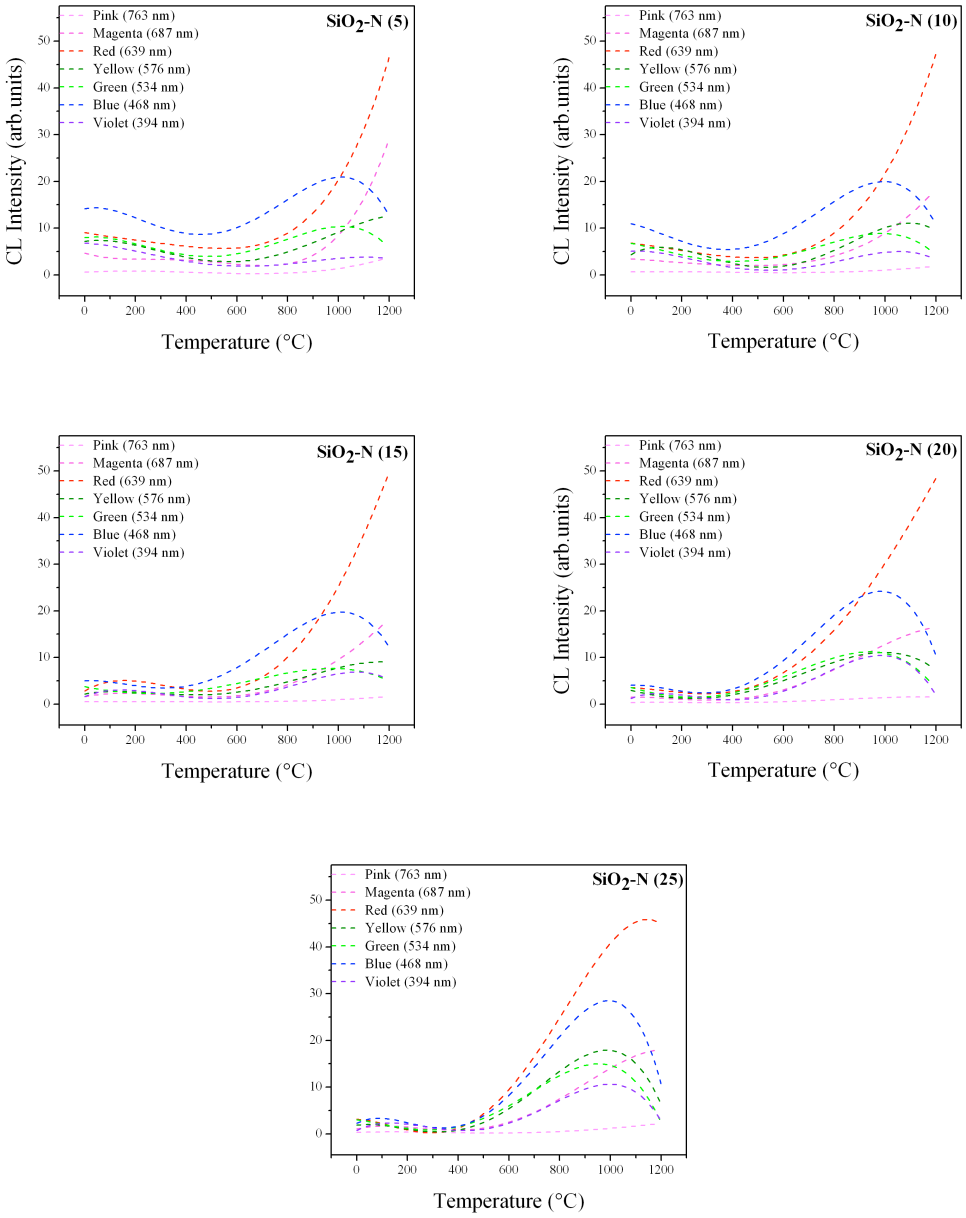

Figure 6.17: *Maximum intensity trend of each bands for SiO_2-N (5), (10), (15), (20), (25) in function of annealing temperature.*

Increasing the concentration of nitrogen, spectra in the annealing temperature of 0-500°C presents a low luminescence emission. Rising up the temperature of thermal treatments, silicon oxynitride structure exhibits strong luminescence bands. Defects in silicon oxynitride has not been subjected to intensive CL investigation. In literature only G. Pezzotti et al. [78] and H. Wong et al. [79] report some characteristic feature of that system. However, it should be expected that the introduction of nitrogen in the matrix, to create oxynitride, form a more complicated network of defects. This is only partially true, as a matter of fact for high annealing temperature the luminescence intensity increase as well as the nitrogen amount in the structure.
However, in the present work, it has been noticed that for as deposited RT synthesized samples the luminescence decrease proportionally with the amount of nitrogen added. Furthermore, as in the pure silica, an initial progressive decreasing of luminescence intensity for annealing up to 500°C is noticed for two of the nitrogen concentration series. To show this features, in figure 6.18 the intensities of ODC and NBOHC related bands for each the composition are plotted in function of the annealing temperature, in the temperature range of 0-500°C.

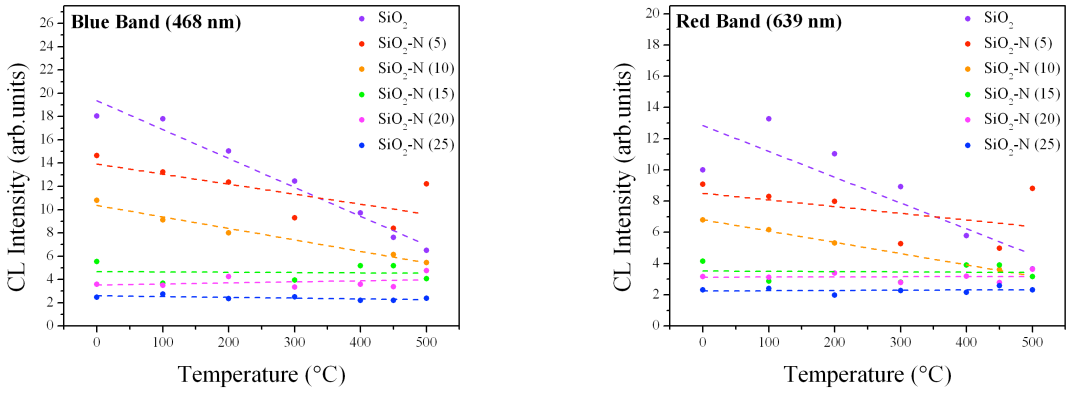

Figure 6.19: *Maximum intensity trend of blue and red bands for each samples in 0-500°C annealing temperature range.*

The luminescence intensity of both red and blue bands decrease with the annealing temperature for SiO_2-N (5), and SiO_2-N (10) and remain constant for SiO_2-N (15), (20), (25). Also, the rate of the intensities decreasing from pure silica to high doped silica. It is possible to assume that the effect of nitrogen doping results in the diminishing of defects in a low annealing temperature range. The absence of ODCs from Si/SiO_2 interface during the annealing of silicon oxynitride in nitrogen atmosphere was also reported by Gritsenko et al. [80], even if the nature of this phenomenon is still unclear. Probably, in this case, the preparation method play a key role in the determination of the final structure. The nitrogen introduced during the deposition reacts with the SiO_2 sputtered from the target and is possible that a twofold coordinated silicon or a non bridging oxygen, both with an unpaired electron, bonds with a nitrogen atom forming oxynitride structure, eliminating the ODC or NBOHC defects centers. As in the un-doped silica, the thermal treatments up to 500°C seem to promote the formation of more stable network, decreasing the density of the defects.

$$2 \equiv SiO\bullet + N_2 \rightarrow \equiv SiON= \tag{6.3}$$

$$3 \equiv Si\text{-}Si\equiv + N_2 \rightarrow 2 \equiv Si_3N \tag{6.4}$$

However, the luminescence of defects related bands starts to grow for annealing temperature higher than 500°C. As a consequence a new feature appears: contrary to the initial range, the luminescence increasing by the increasing of the nitrogen amount in the structure. In comparison with pure SiO_2, the complex network of bonds induced by the nitrogen can lead to the formation of a different kind of defects. The silicon atoms in these defects can be randomly coordinated by different number of nitrogen and oxygen. According to the Mott's rule (eq. 2.3) two possible defect structure originated from silicon, oxygen and nitrogen can be:

$$O_{3\text{-}\beta}N_\beta SiO\bullet \quad \text{or} \quad O_{3\text{-}\beta}N_\beta SiN\bullet \qquad (\beta = 0,\ 1,\ 2\ ,3)$$

The luminescence intensity trend for the bands of each composition in function of the annealing temperature is reported in figure 6.19. The trends reported, are a polynomial interpolation of the effective maximum intensity obtained from the deconvolution analysis, well evidence the change of luminescence behaviour before and after 500°C.

The general explanation for the increased luminescence of the main bands is that the oxynitride structure formed during the deposition above 500°C begins to degrade. This degradation results in the bond-breaking between silicon, oxygen and nitrogen atoms, forming a density of defects higher than that one in the pure silica. Indeed in the red band, where the main luminescence is given by ≡SiO•, a contribute may be due to the ≡Si_2N• defect, or to other under-coordinated form of that defects, which can originates from the rupture of a Si-N bond (6.5) [79]. Indirectly, this defect can influence also the behaviour of STE (6.6), being related by to the threefold coordinated silicon. Moreover, the increasing of the blue band can be due to the recombination of ODCs defects after the thermal treatments in oxidant atmosphere (6.7).

$$\equiv Si_2N\text{-}NSi_2\equiv \rightarrow 2\ \equiv Si_2N\bullet \tag{6.5}$$

$$\equiv Si_2\text{-}N\text{-}Si_2\equiv \rightarrow \equiv Si_2N\bullet + \equiv Si\bullet \tag{6.6}$$

$$\equiv Si\bullet + \bullet Si\equiv \rightarrow \equiv Si\text{-}Si\equiv \tag{6.7}$$

However, the POR associated band (magenta band) increase with a slow rate than the NBHOC. The near-IR band, associated to the interstitial oxygen showing a little variation of intensity, remaining almost constant. In the SiO_2-N (25) it is noticed an intense peak of the yellow band, associated to the impurity, which has been also confirmed by the XPS analysis reported in the following subsection. Furthermore, anomalous behaviour than the general trend has been found in the annealing temperature around 750°C, for the green and the red bands, of each doped samples. Figure 6.20 show the maximum CL intensity for the mentioned bands, of the samples annealed in this range of temperature.

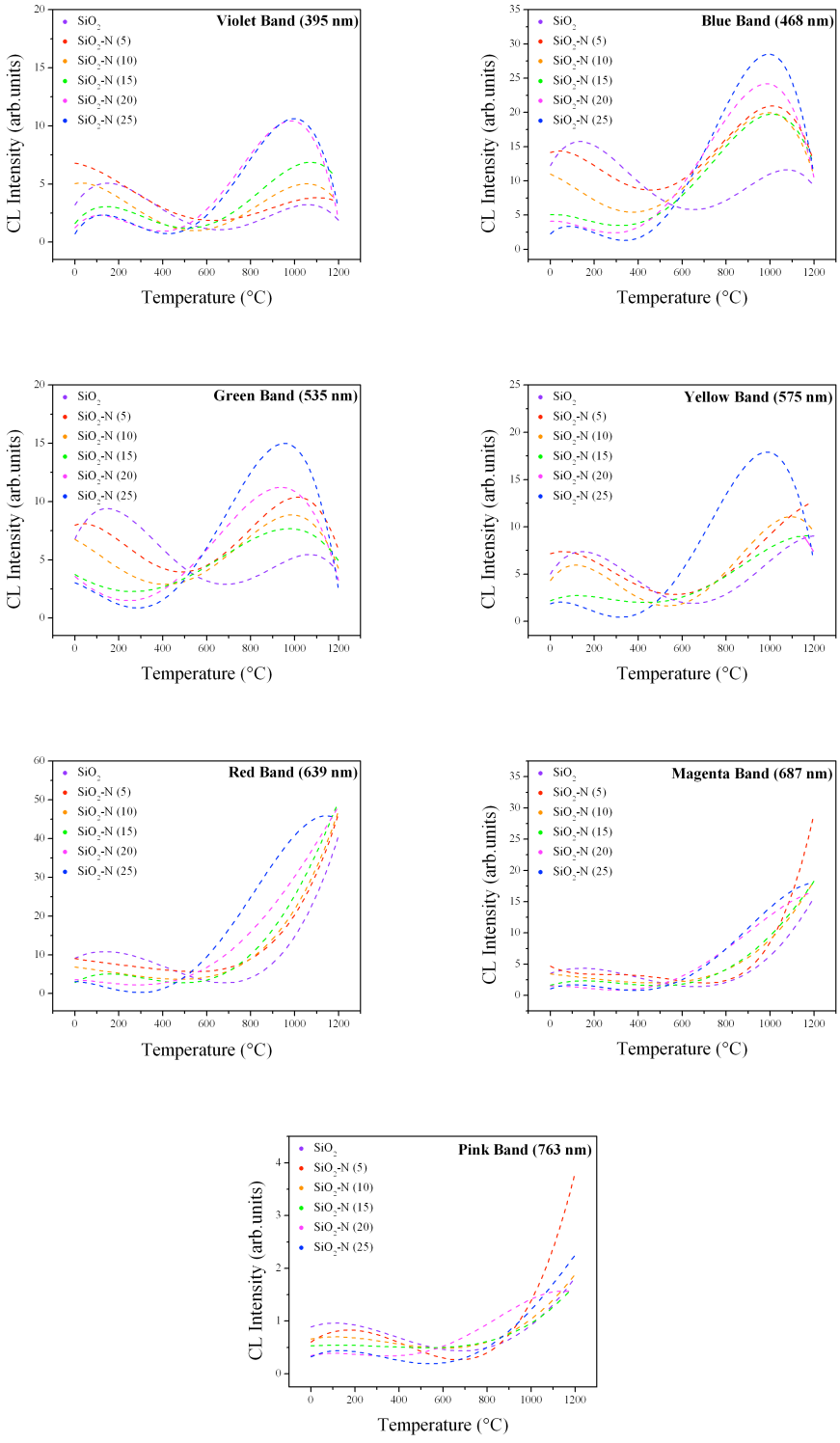

Figure 6.20: *Comparison of maximum intensity trend of each bands for SiO_2-N (5), (10), (15), (20), (25) in function of annealing temperature.*

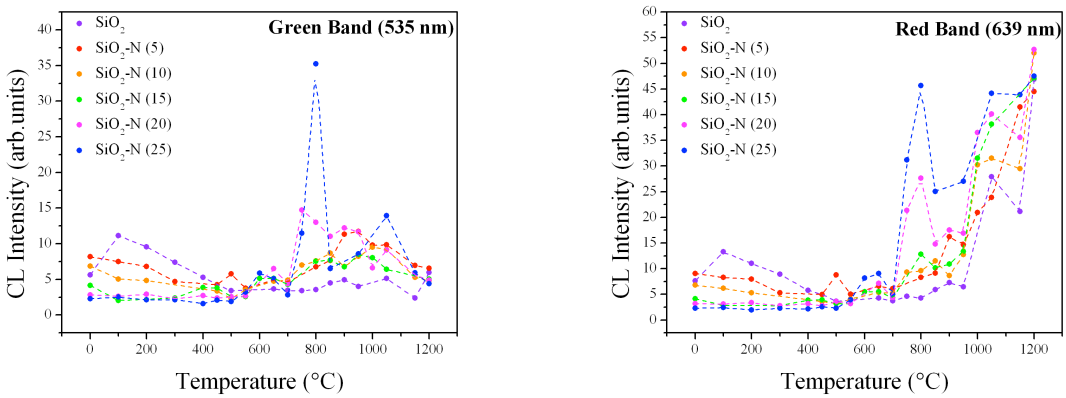

Figure 6.21: *Comparison of maximum intensity green and red band, for SiO_2 and SiO_2-N (5), (10), (15), (20), (25) in function of annealing temperature.*

As reported these bands present a strong luminescence at 800°C, which increase increasing the nitrogen concentration. In different amorphous silica network, such as erbium doped silica, 800°C is the temperature at which the system exhibit the most luminescence intensity due to the rearrangement of erbium site in the matrix [81]. It was also reported that between 750 and 950°C, a tendency of volume contraction in artificial silica glass is observed [75]. The strong luminescence showed by N-SiO_2 samples could be due to a first network reassessment.

Spectra collected above 1000°C annealing of each composition begin to exhibit the same features with comparable luminescence and, at 1200°C show a sets of luminescence bands with the same intensity. This shall indicate that at upon annealing treatments, the nitrogen due to its mobility can escape from the matrix after the oxynitride degradation, and second is a confirm on what stated before: the silica network above the glass transition temperature achieves the equilibrium which induce the same reassessment in each sample, providing a sets of CL bands with the same relative intensities.

6.5 X-ray photoelectron spectroscopy

The chemical change of as deposited N-SiO_2 (25) and samples annealed at 500 and 1050°C were monitored by XPS looking at the silicon $2p$, oxygen $1s$ and nitrogen $1s$ lines. XPS spectra were collected in-depth, sputtering the sample through an 3 keV argon ions gun. The sputtering rate estimated by previous measurement was approximately 1 nm/min. Since no precise information on the samples density is available, the depth profile will be treated in terms of sputtering time.

In figure 6.20 are reported the XPS peaks, collected for silicon, oxygen and nitrogen of each sample, after a 150 minute of sputtering. The silicon $2p$ and oxygen $1s$ lines centered at 532.7 and 103.4 eV of binding energy are characteristic of SiO_2, while the principal nitrogen $1s$ line is located at 398.5 eV, characteristic of SiO_xN_y compounds [82]. Also, a small peak is detectable at 403.5 eV associated to the presence of gaseous species of nitrogen. This peaks vanish inside the silica bulk due to the out-diffusion of nitrogen at high temperature. From a quantitative analysis, XPS indicates that the atomic percentage of nitrogen in as deposit N-SiO_2 (25) bulk is 5%, which is bonded to silicon and oxygen forming silicon oxynitride. Since nitrogen content is lower, no presence of silicon nitride was detected. This observation is in good agreement with RBS results, in which the percentage of nitrogen in the matrix was estimated about 7%. As expected, the intensity of nitrogen $1s$ peak decrease by increasing the annealing temperature, passing from 5% to 1%. What is unexpected, on the basis of CL analysis is that already at 500°C the content of nitrogen decrease significantly. XPS show that the degradation of oxynitride structures probably begins before this temperature. This indicates on one hand that not all the nitrogen bonded in the silica network, participate to the creation of optically active defects, on the other that, despite the nitrogen content, the annealing temperature play a key role in the reassessment of the defects network. Probably annealing in air up to 500°C promotes the formation of stable Si-O-Si bonds, threefold coordinated silicon which is undetectable and gaseous nitrogen:

$$2 \equiv Si_3N + O_2 \rightarrow 2 \equiv Si_2O + 2 \equiv Si\bullet + N_2; \qquad (6.8)$$

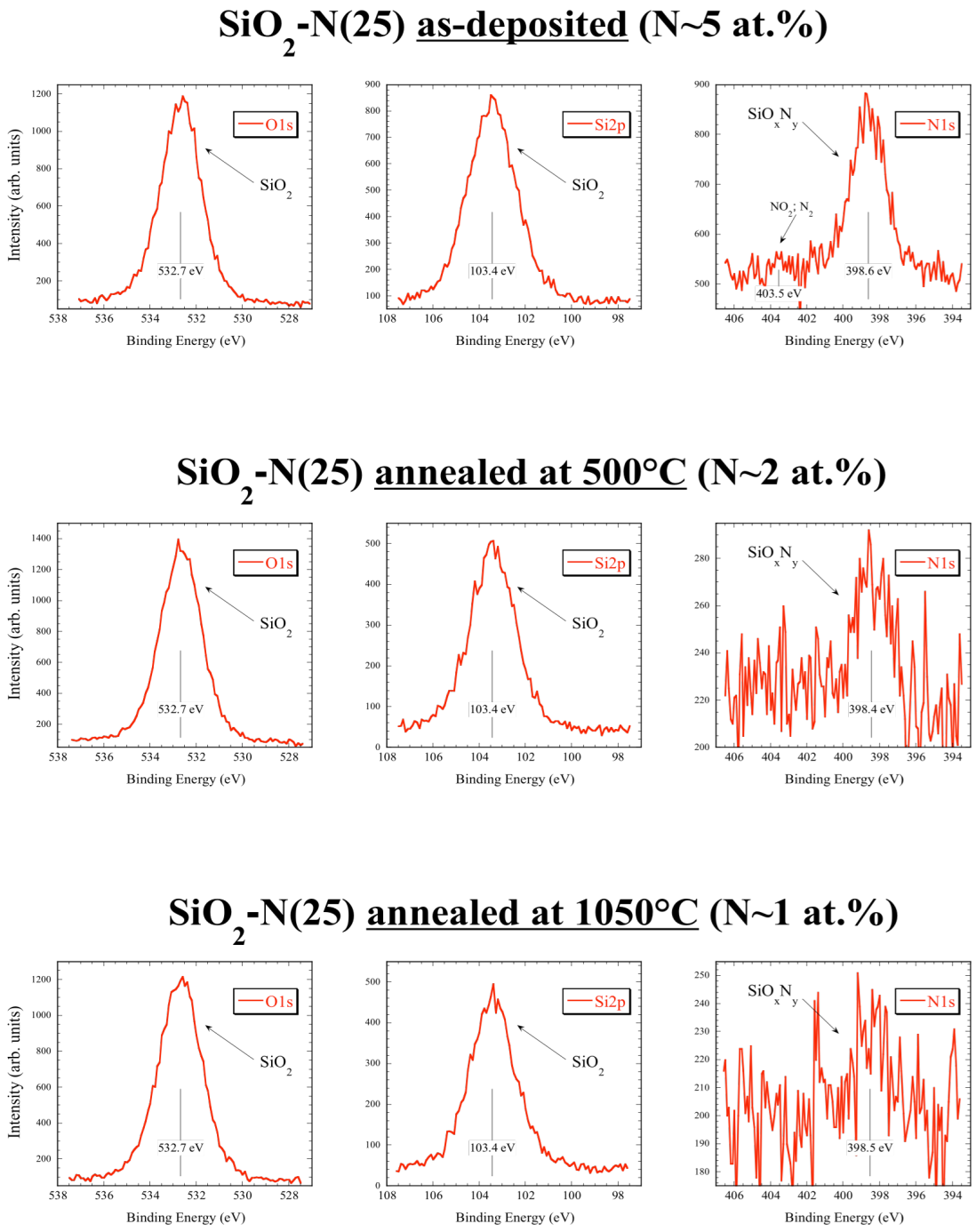

Figure 6.23: *Oxygen 1s, silicon 2p and nitrogen 1s XPS peaks for as deposited, 500 and 1050°C annealed SiO_2-N (25) after 150 min. of sputtering.*

Annealing temperature higher that 500°C lead to the formation of the other mentioned defects, as reported in eq. 6.6.
XPS quantitative analysis also shows that the atomic percentage of silicon and oxygen in SiO_2-N (25) samples is not exactly stoichiometric, showing a lack of silicon. From as deposit to 1050°C the oxygen presence increase, which is consistent with the reaction 6.7. In the figure 6.21 the atomic percentage of silicon, oxygen and nitrogen as a function of the sputtering time for each sample are reported. The common feature present for the two annealed samples is that the atomic percentage of nitrogen increase from the surface into the bulk, while the as deposited sample has the opposite trend. At 1050°C of annealing, nitrogen is almost absent in the layers near the surface, although in as deposited the higher concentration it is found there. The nitrogen percentage in bulk becomes constant approximatively after 100 minute of sputtering in each case.

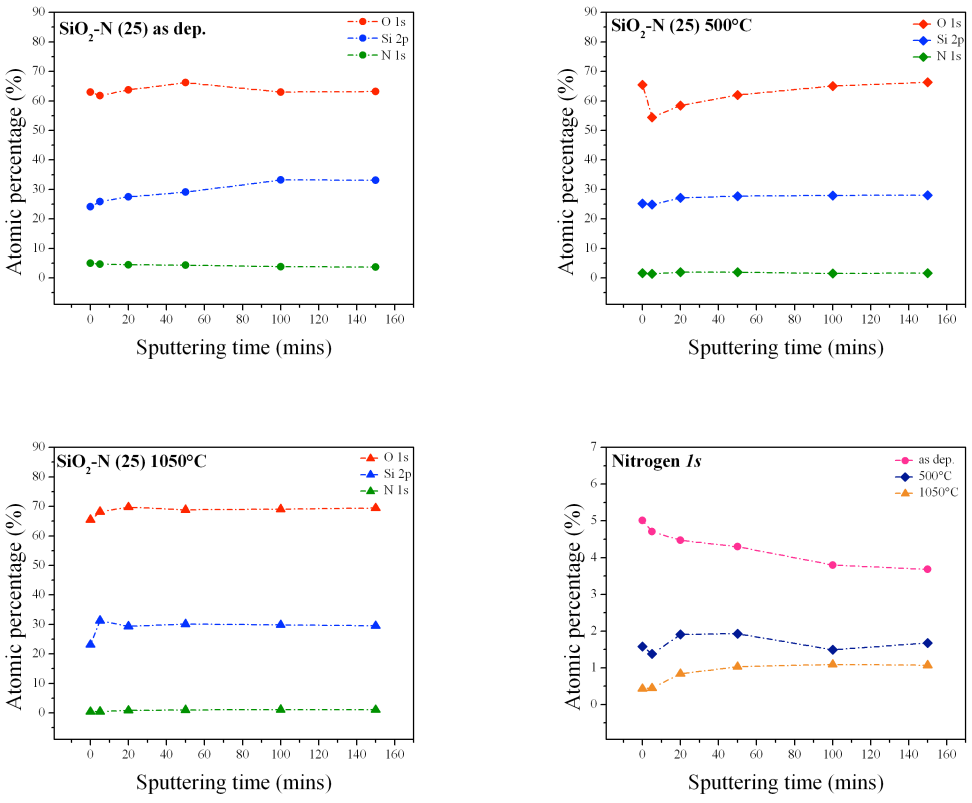

Figure 6.24: *Depth profile of oxygen, silicon and nitrogen for as deposited, 500 and 1050°C annealed SiO_2-N (25).*

6.6 Ion beam induced luminescence

Ion beam induced luminescence (IBIL) is the analysis of visible luminescence produced by solid samples during irradiation with high energetic charged particles. The physical principles on which is based the IBIL technique are very similar to those in CL, except that electronics optical transitions are induced by the secondary electrons scattered into the track by the impinging ion.
The typical energy of the ion beam, to stimulate the luminescence emission, is comprised between 1 and 3 MeV. Since it requires a particles accelerator, this technique was recently developed and, is still unexplored in its full potential.
However, even if this similarity allows to use the CL spectra databases for the analysis of IBIL features arising from different compounds, the two techniques are complementary. Actually the CL, with sensitive equipment is able to analize few nanometers under the surface of a thin film, while IBIL technique can investigate deeply into the bulk, since the penetration range is a function of the beam energy [82-86].

In this thesis, two samples were investigated by means of IBIL: the as deposited SiO_2 and SiO_2-N (25). For each sample, the spectra were recorded monitoring the intensity emission as a function of time. In order to evaluate the evolution of the luminescence band upon irradiation, IBIL spectra were collected every 2 seconds, up to 40 seconds.

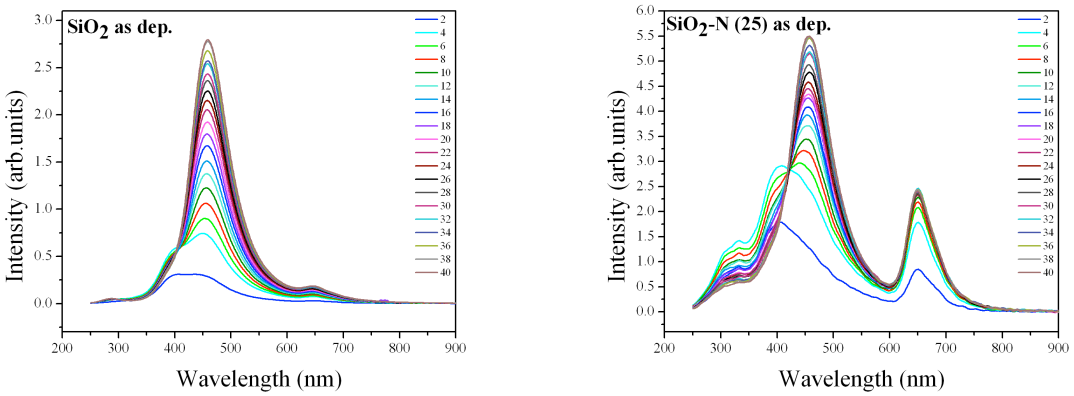

Figure 6.25: *Comparison of IBIL spectra collected with different acquisitions time from SiO_2 and SiO_2-N as dep..*

Both the spectra exhibits some characteristic previously reported in the CL analysis. They present two main peak, one intense at 460 nm, ascribed to the ODC (blue band) and one less intense in at 640 nm associated to NBOHC (red band). Furthermore, it is present a shoulder at 390 nm (more evident in SiO_2-N (25) specimen) assigned to the twofold coordinated silicon (violet bands), and in just for SiO_2-N (25) a new band arose around 320 nm (UV band). It is possible to notice that the relative intensities, for the red and blue bands, are similar to those founds in CL analysis for as deposit samples.
The IBIL profiles, collected for different time of irradiation, shows the structural damage due to the ion beam impact events and, from the comparison between the two spectra, it is evident the modification induced by the nitrogen atom in the matrix. The difference between the specimen becomes clear only after several time of irradiation; in fact IBIL enhances the bands luminescence of SiO_2-N sample greater than in the pure silica. In doped silica, the intensity of NBHOC associated band increase, and after few second of irradiation remain constant, while, in pure silica this band do not show such modification. Also, the shoulder at 390 nm show a different behaviour: in SiO_2-N this band increase first increase, partially overlapping the blue band, then after some seconds decrease until reaching a constant value of intensity. Another consideration can be made on such band: in CL spectra of as deposit samples, especially in the doped one, this shoulder it is not so evident as in IBIL analysis and require a spectral deconvolution to be found. This indicates that the luminescence originated at this position could be associated to a "bulk" luminescence, which is just detectable with the CL. Regarding the ODC associate band, this is the band that undergo to the strongest modification in both of samples, but seem not affected by the nitrogen embedded in the matrix.

Even if the behaviour of the defects upon irradiation is still unclear, from the comparison between their luminescence it is possible recognize the nitrogen contribute. Also, it is possible to notice that the pure silica network is more resistant, than the doped one, to the modification induced from the ion beam.

CL is a suitable technique to study the surface layer of the solid material with high resolution, but is unsuitable to study the bulk features; in this context the IBIL analysis could give an important piece of information.
In this case, in order to give a detailed explanation of the spectrum features, other analyisis are necessary. Anyhow just from this preliminary studies the IBIL is a helpful technique which can contribute to the CL analysis, aiding to found the correlation between the bands and the "hidden" contributes.

Conclusion

In this thesis, an experimental investigation has been presented on nitrogen-doped silica thin films, prepared by RF magnetron sputtering. The experiment was mainly performed by cathodoluminescence (CL) spectroscopy used combining the high scanning flexibility and spatial resolution of the electron probe with a high sensitive detector. Information on the stoichiometry, the chemical state and the dopant amount were also obtained by Rutherford Backscattering Spectroscopy (RBS) and Xray Photoelectron Spectroscopy (XPS) measurements, respectively. Also, Ion Beam Induced Luminescence (IBIL) technique, though based on the same principles of the cathodoluminescence, has been tested for the potential information on the modification of the structure under the ion beam.

The main conclusions are thus summarized:

1) From a comparison with the undoped silica, the nitrogen-doped samples exhibit a reduction in the defects population, towards a more stable structure which is maintained until 500°C of annealing. The amount of the nitrogen is related to the cathodoluminescence bands intensities. In particular, increasing the content of nitrogen, in the temperature range between 0-500°C, the bands luminescence decrease. It seems that the nitrogen introduced during the deposition reacts with a twofold coordinated silicon or a non bridging oxygen eliminating the ODC or NBOHC defects centers.

2) A very interesting feature was observed: all the specimens annealed at 1200°C exhibit a common sets of CL bands, with the same intensity, similar to those collected for specimens of high purity commercial silica. It has been possible to confirm the existing model and propose a new explanation for the mentioned behavior: close to the glass transition temperature a defects distribution is built up in the network, which tends to a "metastable equilibrium", producing a permanent changes of glasses chemical state and inducing the same reassessment in each investigated sample.

3) The CL-based approach has been demonstrated to be particularly suitable to understand on one hand what is the behavior of the silica defects under different thermal treatments and on the other hand what is the role of nitrogen embedded in the structure. Especially the SEM coupled CL of the Ceramic Physics Laboratory in Kyoto Institute of Technology, allows to work in conditions of high spatial resolution in combination with low energy beam, which are necessary to conduct this type of investigation on glassy materials.

4) Facing the defects issue, this study offers preliminary findings that may represent a step forward in the understanding of the doped and undoped silica basic structures, which are fundamentals aiming at realizing advanced materials for solar technology, as well as optoelectronic components. To improve the performance of such devices, a systematic investigation of different silica glass, prepared through different deposition methods, is still required.

Appendix A- Sputter deposition

A.1 Sputter deposition

Sputter deposition, often just called "sputtering", involves the deposition of particles physically (not-thermally) vaporized from a solid surface through the sputtering process. The term sputtering is referred to a physical process in which atoms, ions and molecules are physically ejected from a solid surface, known as "target", by the momentum transfer from an energetic bombarding particle, generally ions with energy in the range of $10^2 \div 10^4$ eV, accelerated from plasma. The bombarding particles can penetrate into the solid target and, through the collision events which causes the transfer of momentum, create a collisional cascade which permits the ejection (sputtering) of the surface target atoms.
The "sputtered" atoms ejected from the target have a wide energy distribution, up to ten's of electronvolts, and can be used to grow the films onto a substrate appropriately positioned. Sputtering is just one of the several processes that occur when an energetic particle strikes the atoms of the target surfaces. The interaction between an energetic particle and the solid surface can also lead to defects formation, ion implantation or channeling, as illustrated in figure A.1.

There are many advantages of using sputtering deposition in comparison with other physical and not-physical deposition techniques, in particular the enhanced features of the sputtered films, such improved hardness and adhesion to the substrate, and the possibility to obtain co-deposited and multilayer films. Even if the availability of many parameters to control sputter deposition

make it a complex process, a large degree of control over the film properties is allowed which make this deposition a suitable technique to fabricate high quality material for electronic and optical industry.

The most common sputter deposition is the plasma-based sputtering, but many configurations of this were developed. From the first planar cathode configuration, nowadays more complex system, which use radiofrequency and magnetic fields, are available [36].

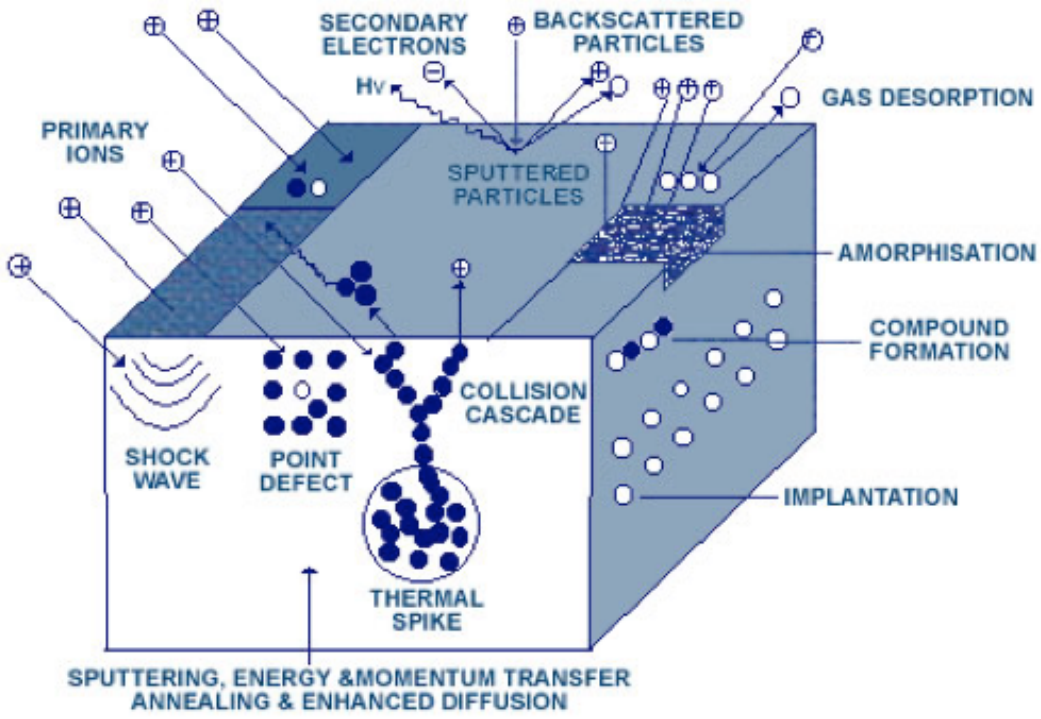

Figure A.1: *Representation of collisional events at the target surface.*

A.2 DC diode sputtering

The cathode DC diode sputtering is a simple configuration of plasma sputtering, through which is possible to understand the basic phenomena involved in the sputtering deposition. In this configuration, there are two parallel planar electrode into a high vacuum chamber: the cathode electrode is the sputtering target (normally cooled with water) while the substrate is placed on the anode which is at ground potential, as shown in figure A.2. The chamber under high vacuum (10^{-6}-10^{-7} mbar) is filled with the working gas, usually noble gas such argon, krypton and xenon, because they are inert and can easily ionize. A continuous potential is applied between the two electrodes for accelerating the electrons from the cathode to the anode, and in order to ionize the working gas through the collision with its particles.

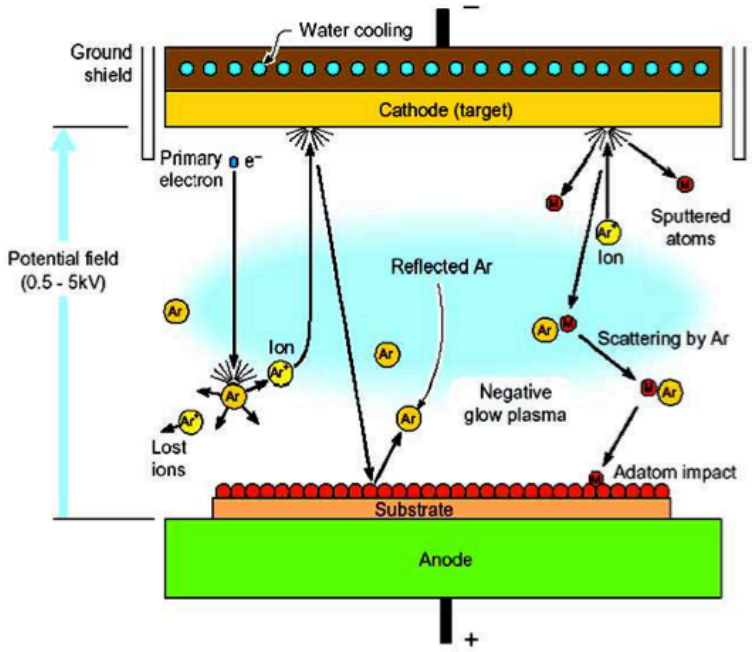

Figure A.2 : *DC planar diode configuration.*

For obtaining the ionization of the gas it is necessary to have an appropriate pressure in the chamber: if it is too low the electron can reach the anode without colliding with the gas atoms, while if it is too high the electrons does not increase sufficiently their kinetic energy before the collision with the particles.

When the first electron strikes an atom of the gas, with sufficient energy for ionizing them, an ion and a secondary electron are produced which are respectively accelerated to the cathode and to the anode. The collision between the ion and the target surface cause the ejection of secondary electrons, which are accelerated back away from the cathode. These high energetic particles collide with gas atoms creating ions which feed the process of plasma formation, which is started above a certain value of discharge potential. If the secondary electrons produce a number of ions as many as those that are neutralized at the cathode, then the plasma is sustained.
This is a dynamic equilibrium in which the body of the plasma is neutral. Because of the different velocity of both electrons and ions, in regions close to the electrodes a positive space charge, called plasma sheats, is developed and the plasma potential is higher than the potential of any surfaces in electrical contact with the plasma. For this reason, the electric field is constrained between these two positive space charge regions. If the colliding ions have sufficient energy, atoms from the target surface can be ejected, or "sputtered", and deposited onto a substrate forming the film. Some of the ions may be neutralized by charge-exchange processes, producing high energetic neutral particles, which are not affected by the electric field and may bombard the non-electrode surface causing sputtering and films contamination. The cathode in the DC diode configuration must be an electrically conductive material, since a dielectric cathodic surface can develop positively charged surface, which prevents the ion bombardment and cause the extinction of the discharge.

An advantage of this configuration is that plasma can be established uniformly over a large area, so the target surface not need to be shaped to be conformal to the substrate shape, but is used only to deposit simple conductive materials. The DC diode sputtering present some disadvantage, such the lower rate of deposition due to the limited number of collision that ionize the working gas, and the overheating of the substrate caused by the extensive electron bombardment. The development of magnetron sputtering improved both these critical aspects.

Appendix B- RBS

The Rutherford backscattering spectroscopy (RBS) is a technique used for the quantitative analysis of the composition, thickness and depth profiling of thin solid films or surface near-regions of bulk materials.
It is based on the detection of light ions elastically backscattered by the nuclei of atoms in the specimen.

B.1 Basic principles

In an RBS analysis the surface of a target specimen placed in vacuum is irradiated with a beam of mono-energetic ions, usually H^+ or He^+ with energy in the range of 0.5 to 2.5 MeV. As a results of the collision with the target atom, heavier than the impinging ion, the light ion are backscattered and detected (fig B.1a). In the backscattering interaction, considered as elastic collision (fig. B.1b), energy is transferred from the ion to the stationary target atom. The energy ratio between the impinging particle energy E_1 after collision and its energy E_0 is given by:

$$K = \frac{E_1}{E_0} = \left[\frac{M_1 \cos\theta - \sqrt{M_2^2 - M_1^2 \sin^2\theta}}{M_1 + M_2} \right]^2 \qquad \text{(B.1)}$$

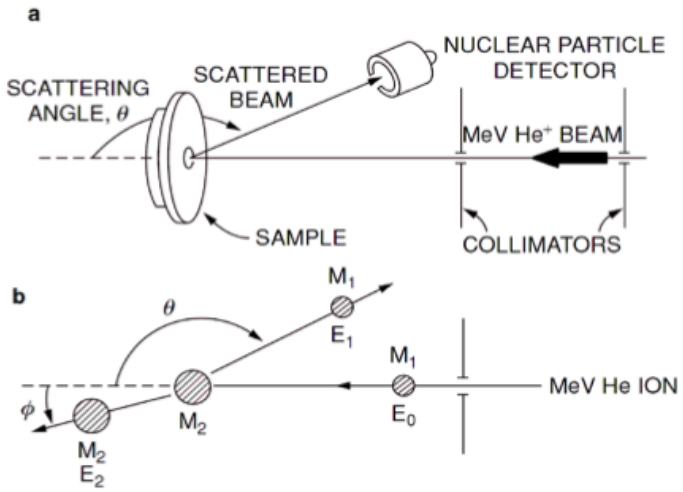

Figure B.1: *Schematic representation of (a) RBS apparatus and (b) scattering geometry.*

The energy ratio, called the kinematic factor K, shows that the energy after scattering depends only on the mass M_1 of the projectile, the mass M_2 of the target atom, and the scattering angle ϑ (i.e., the angle between the incident and scattered beams). If M_1, E_0, and ϑ are known, then M_2 may be determined and the target element identified.

B.2 Instrumentation

RBS equipment typically consists in an particle accelerators. The ions are first produced in an ion source, then electrostatically accelerated, usually with a Van de Graaf accelerator. Since the ions are normally in different charge states, to extract a beam suitable for materials analysis, the beam is first passed into the field of an analyzing magnet where the ions are selected on their selected on the mass-charge ratio. The beam obtained steered to the target by electrostatic or magnetic lenses. The detection of backscattered ions is usually performed using a solid-state detector

Appendix C- XPS

The X-ray photoelectron spectroscopy, also called ESCA, is one of the most used surface characterization methods and consist in the irradiation of a surface with x-ray photons which cause the emission of photoelectrons from surface atoms (figure C.1).

C.1 Basic principles

When a photon, with energy hv, collides with an electron with binding energy E_B, the entire photon energy is transferred to the electron and an emitted photoelectrons with kinetic energy E_k is ejected. Considering the work-energy function terms, Φ_s the kinetic energy is given by:

$$E_k = hv - E_b - \Phi_s \tag{C.1}$$

E_B is the kinetic energy associated to the shell from which the electron is ejected. The electron may come from a core level or from the occupied portion of a valence band, but in XPS measurement the attention is focused on the electron in core-levels. The measured kinetic energy of the emitted photoelectron leads to an elemental analysis because no two elements have the same set of electronic binding energy. Depending on the electronegativity of the atoms involved in a chemical bond, the electron cloud surrounding them is slightly shifted towards the more electronegative one. For the photoelectrons coming from the internal shells this induces an additional energy gap to overcome if emitted from the atom less electronegative: in this case the binding

energy will be slightly larger. This small but detectable shift allow to have information on the chemical state of the atoms involved.
The value of binding energy for most of the elements present in the periodic

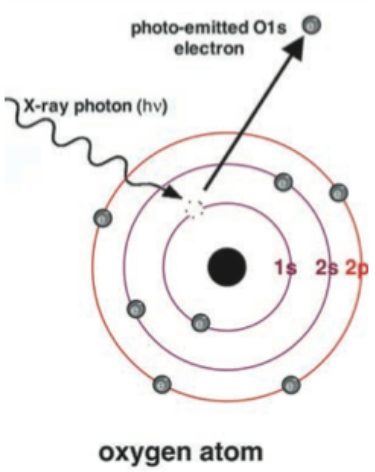

Figure C.1: *Representation of the photoelectrons emission.*

table are reported in literature, except for hydrogen and helium that cannot be detected because of their low cross-section of interaction.

C.2 Instrumentation

The instrumental apparatus for an XPS measurement schematically showed in fig C.2, consist in a high vacuum chamber (pressure range in the order of 10^{-8} Pa) where a x-ray source and an electron energy analyzer are placed.
The vacuum requirements of the chamber is in the order of 10^{-8} Pa because of this technique, sampling a few atom layers, is very sensitive to surface contamination, most of which comes from the residual gases in the vacuum system.
The x-ray source is chosen considering its resolution, because for extract detailed information of an individual elemental photoelectron spectra, an energy resolution better than 1 eV is needed. The final resolution depends on

the width of the energy level from which the photoelectron comes, on the linewidth of the X-ray source, and on the analyzer contribution.
Among the characteristic x-ray line of a few material Mg_{ka} and Al_{ka} are generally used. This is due to their line energies and their width that are 1253.6 nm with 0.7 eV of width and 1468.6 nm with 0.85 eV of width, respectively for Mg_{ka} and Al_{ka}.

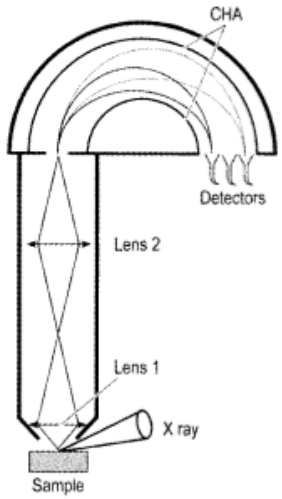

Figure C.2: *Representation of a CHA analyzer.*

The measurement of the photoelectron energy is usually made with a concentrical hemispherical analyzer (CHA), placed in between the collection lenses and the detector

C.2.1 Depth profiling

It is possible to obtain in-depth information by removing part of the surface material before a new XPS investigation. This can be performed through sputtering induced by an ion bombardment of the sample surface, using an ion gun. Usually the depth profiling is allowed by a low energy sputtering (3-5 keV) with a noble gas such Ar, to minimize the physical-chemical effects related to the ion bombardment.

Appendix D- IBIL

The Ion beam induced luminescence technique is based on the study of the light emitted by solid samples in the visible and ultra violet range of the electromagnetic spectrum. The luminescence, generated by the incidence of an ion beam (H^+, He^+), is related to the transitions of the outermost electrons involved in chemical bonds of atoms or in network defects.

D.1 Basic principles

The basic principles of IBIL as an analytical technique are very similar to those explained in chapter 4 for cathodoluminescence.
However, since the energy of the ion beam is comprised between 1 and 3 MeV, the electronic optical transitions are induced by the secondary electrons scattered into the track by the impinging ion. IBIL technique is able to probe a specimen relatively uniformly up to 20 microns below the surface and is sensitive to the local chemical environment of compounds, trace substitutes and to the microstructure of the network.
The IBIL apparatus consists in a particle accelerator. The ion beam appropriately selected impact on sample placed in a vacuum chamber. The light emitted from the sample is collected by a optical fibres and transmitted to a spectrometer. Then the various intensity detected as a function of wavelength are recorded by a CCD detector. The spectral acquisition time, typically comprised between 1 and 20 second, depends on the intrinsic luminescence of the sample probed and the characteristics of the incident beam.

References

[1] Markvart, T., and Castaṇer, L. (2003). Practical handbook of photovoltaics fundamental and applications: solar cells. Elsevier Science.

[2] Wenham, S. R. (1993). Buried-contact silicon solar cells. *Progress in Photovoltaics*: *Research and Applications, 1 ,* 3-10.

[3] Wang, Y., Cheng, X., Lin, Z., and Zhang, C. (2003). Optimization of PECVD silicon oxynitride films for anti-reflection coating. *Vacuum*, *72,* 345-349.

[4] Lipinski, M., Kaminski, A., Lelièvre, J. F., Lemiti, M., Fourmond, E., and Zieba, P. (2007). Investigation of graded index SiOxNy antireflection coating for silicon solar cell manufacturing. *Physica Status Solidi (c)*, *4*, 1566–1569

[5] Ghandhi, S. K. (2008). VLSI fabrication principles: silicon and gallium arsenide. Wiley-India.

[6] Shibata, N. (1991). Plasma-chemical vapor-deposited silicon oxide/ silicon oxynitride double-layer antireflective coating for solar cells. *Japanese Journal of Applied Physics, 30,* 997-1001.

[7] Richards, B. (2004). Comparison of TiO_2 and other dielectric coatings for buried-contact solar cells: a review. *Progress in Photovoltaics: Research and Applications*, *12*, 253–281.

[8] Wenham, S., Zhao, J., Dai, X., and Wang, A. (2001). Surface passivation in high efficiency silicon solar cells. *Materials and Solar Cells*, *65*, 377-384.

[9] Leguijt, C., and Eikelboom, J. (1996). Low temperature surface passivation for silicon solar cells. *Materials and Solar Cells*, *40*, 297-345.

[10] Serenyi, M., Racz, M., and Lohner, T. (2001). Refractive index of sputtered silicon oxynitride layers for antireflection coating. *Vacuum*, *61*, 245–249.

[11] Tryggve, B. (1982). Silicon oxynitride; a material for GRIN optics, *Applied Optics, 21,* 1069-1072

[12] Ebong, A., Taouk, M., Honsberg, C., and Wenham, S. (1996). The use of oxynitrides for the fabrication of buried contact silicon solar cells. *Solar energy Materials and Solar Cells*, *40*, 183–195.

[13]Moore, G. (1965). Cramming More Components onto Integrated Circuits, *Electronics Magazine*, 38, 114-117.

[14] Hitz, B. (2009). Intel turns to photonics to extend Moore's law. *Physics World*. 12-13

[15] Soref, R. (2005). Silicon photonics technology: past, present and future. *Proceeding SPIE* , *5730*, 19–28.

[16] Khriachtchev, L. (2008). *Silicon nanophotonics: basic principles, present status and perspectives*. Pan Stanford Pub.

[17] de Ridder, R. M., Warhoff, K., Driessen, A., Lambeck, P. V., and Albers, H. (1998). Silicon oxynitride planar waveguiding structures for application in optical communication. *Selected Topics in Quantum Electronics, IEEE Journal of*, *4*, 930–937.

[18] Bayliss, S., and Gurman, S. (1994). Silicon oxynitride as a tunable optical material. *Journal of Physics: Condensed Matter*, *6*, 4961-4970.

[19] Rand, M. J., and Standley, R. D. (1972). Silicon oxynitride films on fused silica for optical waveguides. *Applied Optics*, *11*, 2482-2488.

[20] Wong, H. (2002). Recent developments in silicon optoelectronic devices. *Microelectronics Reliability*, *42*, 317-326.

[21] Sun, F., and Driessen, A. (2010). High performance optical waveguides based on boron and phosphorous doped silicon oxynitride. *Proceeding SPIE, 7604.*

[22] Gorecki, C. (2000). Optimization of plasma-deposited silicon oxinitride films for optical channel waveguides. *Optics and Lasers in Engineering*, *33*, 15-20.

[23] Del Giudice, M., Bruno, F., and Cicinelli, T. (1990). Structural and optical properties of silicon oxynitride on silicon planar waveguides. *Applied optics*, *29,* 3489-3496.

[24] Worhoff, K., Driessen, A., Lambeck, P. V., Hilderink, L. T. H., Linders, P. W. C., and Popma, T. J. A. (1999). Plasma enhanced chemical vapor deposition silicon oxynitride optimized for application in integrated optics. *Sensors And Actuators A: Physical*, *74,* 9-12.

[25] Driessen, A., Hoekstra, H., Blom, F., and Horst, F. (1998). Evaluation of polymer based third order nonlinear integrated optics devices. *Optical Materials*, *9,* 329-333.

[26] Blom, F. C., van Dijk, D. R., Hoekstra, H. J. W. M., Driessen, A., and Popma, Th. J. A. (1997). Experimental study of integrated-optics microcavity resonators: Toward an all-optical switching device, *Applied Physics Letters, 71,* 747–749.

[27a] Ryall, W. (1969). Silicon oxynitride stability. *Science*, (9), 1363-1364.

[28b] Xu, Y., and Ching, W. (1995). Electronic structure and optical properties of α and β phases of silicon nitride, silicon oxynitride, and with comparison to silicon dioxide. *Physical Review B*, *51*(24), 379-389.

[29] Hillert, M., and Jonsson, S. (1992). Thermodynamic Calculation of the Si-N-O System. *Zeitschrift fur Metallkunde, 83,* 648-654.

[30] Gritsenko, V., Xu, J., Kwok, R., and Ng, Y. (1998). Short range order and the nature of defects and traps in amorphous silicon oxynitride governed by the Mott rule. *Physical review letters*, (100), 3-6.

[31] Scopel, W., Fantini, M. C., Alayo, M., and Pereyra, I. (2002). Local structure and bonds of amorphous silicon oxynitride thin films. *Thin Solid Films*, *413*(1-2), 59-64

[32] Kroll, P. (2005). A DFT study of amorphous silicon oxynitride. *Journal of Non-Crystalline Solids*, *351*(12-13), 1127-1132.

[33] Nassau, K. (2001). The physics and chemistry of colour, 2nd ed., Wiley-Interscience.

[34] Nalwa, H. S. (2001). *Silicon based materials and devices* (Vol. 2). Academic Press.

[35] Pezzotti, G., and Leto, A. (2009). Contribution of Spatially and Spectrally Resolved Cathodoluminescence to Study Crack-Tip Phenomena in Silica Glass. *Physical Review Letters*, *103*, 1-4.

[36] Mattox, D. M. (2010). Handbook of physical vapor deposition (PVD) processing: film formation, adhesion, surface preparation and contamination control. Noyes Publications.

[37] Holt, D. B., and Yacobi, B. (2007). Extended defects in semiconductors: electronic properties, device effects and structures. 1st ed., Cambridge University Press.

[38] Holt, D. B., and Yacobi, B. (1990). Cathodoluminescence microscopy of inorganic solids. 1st ed., Plenum Press.

[39] Pankove J. I., (1971). Optical processes in semiconductors. 1st ed., Dover Publications.

[40] Burns, R. (1970). Mineralogical Applications of Crystal Field Theory, 1st ed. Cambridge University Press.

[41] Gucsik, A. (2009). Cathodoluminescence and its Application in the Planetary Sciences. Springer.

[42] Everhart, T. E., Hoff, P. H., (1971). Determination of kilovolt electron energy dissipation vs penetration distance in solid materials. *Journal of Applied Physics*, *42,* 5837-5846.

[43] Goldstein, J. (2003). Scanning electron microscopy and X-ray microanalysis. 3rd ed., Plenum.

[44] Kanaya, K., and Okayama, S. (1972). Penetration and energy-loss theory of electrons in solid targets. *Journal of Physics D: Applied Physics*, *5*, 43-58.

[45] Yacobi, B. (1986). Cathodoluminescence scanning electron microscopy of semiconductors. *Journal of Applied Physics*, *59*, 15-39.

[46] Remond, G., Cesbron, F., Chapoulie, R. (1992). Cathodoluminescence applied to the microcharacterization of mineral materials: a present status in experimentation and interpretation. *Scanning Microscopy, 6,* 23-68.

[47] Gritsenko, V. a., Svitasheva, S. N., Petrenko, I. P., Novikov, Y. N., Morokov, Y. N., Wong, H., Kwok, R. W. M., (1998). Characterization of the silicon nitride–thermal oxide interface in oxide–nitride–oxide structures by ELS, XPS, ellipsometry, and numerical simulation. *Microelectronics Reliability, 38*, 745-751.

[48] Liu, Y., Lin, I., and Zhang, X. (2008). Mechanical properties of sputtered silicon oxynitride films by nanoindentation. *Materials Science and Engineering A, 489*, 294-301.

[50] Price, K. J., McNeil, L. E., Suvkanov, A., Irene, E. a., MacFarlane, P. J., and Zvanut, M. E. (1999). Characterization of the luminescence center in photo- and electroluminescent amorphous silicon oxynitride films. *Journal of Applied Physics, 86,* 2628-2637.

[51] Stadler, a., Genchev, I., Bergmaier, a., Dollinger, G., Petrova-Koch, V., Hansch, W., Baumgärtner, H., et al. (2001). Nitrogen implantations for rapid thermal oxinitride layers. *Microelectronics Reliability, 41*, 977-980.

[52]He, L. (2002). Properties of amorphous SiO_2 films prepared by reactive RF magnetron sputtering method. *Vacuum*, *68*, 197-202.

[53] Rebib, F., Tomasella, E., Dubois, M., Cellier, J., Sauvage, T., and Jacquet, M. (2005). Structural and optical investigations of SiON thin films deposited by R.F. sputtering. *Surface and Coatings Technology*, *200*, 330-333.

[54] Pinard, L., and Mackowski, J. M. (1997). Synthesis and physicochemical characterization of silicon oxynitride thin films prepared by rf magnetron sputtering. *Applied Optics*, *36*, 5451-5460.

[55] Pinard, L. (1998). Optical losses of multilayer stacks synthesized with silicon oxynitride by r.f. magnetron sputtering. *Thin Solid Films*, *333*, 126-133.

[56] Battaglin, G., Cattaruzza E., Gonella F., Polloni R., Scremin B.F., Mattei G., Mazzoldi P., Sada C. (2004). Structural and optical properties of Cu:silica nanocomposite films prepared by co-sputtering deposition, *Applied Surface Science, 226*, 52-56.

[57] Cattaruzza E., Battaglin, G., Gonella F., Polloni R., Scremin B.F., Mattei G., Mazzoldi P., Sada C., Au–Cu nanoparticles in silica glass as composite material for photonic applications, *Applied Surface Science, 254,* 1017-1021.

[58] Thornton, J. A., (1986). The microstructure of sputter-deposited coatings. *Journal of Vacuum Science and Technology A: Vacuum, Surfaces, and Films*, 4, 3059-3065.

[59] Shelby, J. (2005). Introduction to glass science and technology. 2nd ed., RCS.

[60] Leto, A., Munisso, M. C., Porporati, a A., Zhu, W., and Pezzotti, G. (2008). Stress dependence of paramagnetic point defects in amorphous silicon oxide. *The journal of physical chemistry A, 112*, 3927-3934.

[61] Skuja, L. (1998). Optically active oxygen-deficiency-related centers in amorphous silicon dioxide. *Journal of Non-Crystalline Solids, 239*, 16-48.

[62] Salh, R., (2011) Defect related luminescence in silicon dioxide network: a review, *Crystalline Silicon - Properties and Uses*, ed. Sukumar Basu, InTech, 136-172.

[63] Tohmon, R., Shimogaichi, Y., Mizuno, H., Ohki, Y., Nagasawa, K., and Hama, Y. (1989). 2.7-eV luminescence in as-manufactured high-purity silica glass. *Physical Review Letters*, 62, 1388–1391.

[64] Skuja, L., and Entzian, W. (1986). Cathodoluminescence of Intrinsic Defects in Glassy SiO_2, Thermal SiO_2 Films, and α-Quartz. *Physica Status Solidi (a)*, *191*, 191-198.

[65] Nishikawa, H., Shiroyama, T., Nakamura, R., Ohki, Y., Nagasawa, K., and Hama, Y. (1992). Photoluminescence from defect centers in high-purity silica glasses observed under 7.9-eV excitation. *Physical Review B, 45*, 586-591.

[66] Skuja, L. (1989). Comment on "Luminescence of fused silica: Observation of the O^{2-} emission band. *Physical Review B*, *39*, 3909-3911.

[67] Imai, H., Arai, K., Imagawa, H., Hosono, H., and Abe, Y. (1988). Two types of oxygen deficient centers in synthetic silica glass. *Physical Review B*, *38*, 12772-12775.

[68] Jones, C. E., Embree, D. (1976). Correlations of the 4.77–4.28-eV luminescence band in silicon dioxide with the oxygen vacancy. *Journal of Applied Physics, 47,* 5365-5370.

[69] Pacchioni, G., and Ierańo, G. (1998). Ab initio theory of optical transitions of point defects in SiO_2. *Physical Review B*, *57*, 818-832.

[70] Nishikawa, H., Watanabe, E., Ito, D., and Ohki, Y. (1994). Decay Kinetics of the 4.4 eV Photoluminescence Associated with the Two States of Oxygen-Deficient-Type Defect in Amorphous SiO_2. *Physical review letters, 72,* 2101–2104.

[71] Pacchioni, G., Ieranò, G., and Márquez, A. (1998). Optical Absorption and Nonradiative Decay Mechanism of E′ Center in Silica. *Physical Review Letters, 81*, 377-380.

[72] Munekuni, S., Yamanaka, T., Shimogaichi, Y., Tohmon, R., Ohki, Y., Nagasawa, K., and Hama, Y. (1990). Various types of nonbridging oxygen hole center in high-purity silica glass. *Journal of Applied Physics, 68*, 1212-1217.

[73] Fitting, H. (2001). Cathodoluminescence of crystalline and amorphous SiO2 and GeO2. *Journal of Non-Crystalline Solids, 279*, 51-59.

[74] Shluger, A. (1990). Models of the self-trapped exciton and nearest-neighbor defect pair in SiO_2. *Physical Review B, 42*, 9664-9673.

[75] Bruckner, R. (1970). Properties and structure of vitreous silica. I. *Journal of Non-Crystalline Solids*, *5*, 123-175.

[76] Salh, R., Vonczarnowski, a, and Fitting, H. (2007). Cathodoluminescence of non-stoichiometric silica: The role of oxygen. *Journal of Non-Crystalline Solids, 353*, 546-549.

[77] Salh, R., von Czarnowski, a., Zamoryanskaya, M. V., Kolesnikova, E. V., and Fitting, H.-J. (2006). Cathodoluminescence of SiO_x under-stoichiometric silica layers. *Physica Status Solidi (a), 203*, 2049-2057.

[79] Pezzotti, G., Hosokawa, K., Munisso, M. C., Leto, A., and Zhu, W. (2007). Stress dependence of optically active diamagnetic point defects in silicon oxynitride. *The Journal of Physical Chemistry A*, *111*, 8367-8373.

[79] Wong, H. (2002). Defects in silicon oxynitride gate dielectric films. *Microelectronics Reliability, 42*, 597-605.

[80] Gritsenko, V. (1999). Cathodoluminescence and photoluminescence of amorphous silicon oxynitride. *Microelectronics and Reliability*, *39*, 715-718.

[81] Gonella. F, Battaglin G., Cattaruzza E., Trave E., Leto A., and Pezzotti, G. (2012). Temperature-driven local rearrangement in the Er environment of Er-doped silica glass films prepared by rf-cosputtering deposition, *Thin Solid Films, 520,* 4758-4761

[82] Mazzoldi, P., Carnera, A., Caccavalle, F., Favaro, M.L., Boscolo-Boscoletto, A., Granozzi, G., Bertoncello, R., Battagli, G. (1991). N and Ar ion-implantation effects in SiO_2 films on single-crystal substrates. *Journal of Applied Physics, 70,* 3528-3536.

[83] Brooks, R. J., Hole, D. E., Townsend, P. D., & Wu, Z. (2002). Ion beam induced luminescence of thin films. *Nuclear Instruments and Methods in Physics Research Section B: Beam Interactions with Materials and Atoms, 190*, 709-713.

[84] Brooks, R. J., Hole, D. E., & Townsend, P. D. (2002). Ion beam induced luminescence of materials. *Nuclear Instruments and Methods in Physics Research Section B: Beam Interactions with Materials and Atoms*, *190,* 136-140.

[85] Quaranta, a., Vomiero, a., Carturan, S., Maggioni, G., & Della Mea, G. (2002). Polymer film degradation under ion irradiation studied by ion beam induced luminescence (IBIL) and optical analyses. *Nuclear Instruments and Methods in Physics Research Section B: Beam Interactions with Materials and Atoms, 191*, 680-684.

[86] Quaranta, a., Salomon, J., Dran, J. C., Tonezzer, M., & Della Mea, G. (2007). Ion beam induced luminescence analysis of painting pigments. *Nuclear Instruments and Methods in Physics Research Section B: Beam Interactions with Materials and Atoms, 254*, 289-294.

Acknowledgements

Innanzitutto, per la possibilità di svolgere questo lavoro fatto in collaborazione con il Kyoto Institute of Technology (Giappone), per la fiducia dimostratami oltre che per l'aiuto ricevuto durante lo sviluppo di questa tesi, sento di dover ringraziare vivamente il Prof. Franceso Gonella, con il quale spero tanto di poter collaborare anche nei prossimi anni a venire.
Un doveroso ringraziamento va al Prof. Giuseppe Pezzotti del Kyoto Institute of Technology, il quale ospitandomi nel suo gruppo di ricerca (per ben 3 mesi!!) e fornendo i mezzi tecnologici e logistici, ha reso possibile questa fantastica collaborazione tra due realtà di ricerca, permettendomi di sviluppare al meglio il lavoro di tesi. Inoltre, devo ringraziarlo di cuore sopratutto per avermi dato la possibilità di continuare il proseguo dei miei studi nel dipartimento sotto la sua direzione.
Un ringraziamento speciale va al Dr. Andrea Leto (al quale devo molto), non solo per avermi dato una grande mano con le misure sperimentali, ma sopratutto per essersi preso cura di me durante il mio periodo in Giappone.
Grazie infinite anche al Dr. Leonardo Puppilin per l' aiuto scientifico, per le tante serate passate insieme in Giappone e per le piacevoli discussioni sulla serie A (sopratutto quando vinceva la Juve).
Una parte sostanziale di ringraziamenti vanno sopratutto al Dr. Elti Cattaruzza e al Dr. Enrico Trave, i quali sempre con cordialità e disponibilità, hanno dedicato parte del loro tempo per aiutarmi nella preparazione dei campioni, nella discussione dei dati sperimentali e redazione della tesi.

Un caloroso ringraziamento va a Michele Back, amico fidato con il quale ho condiviso questa mitica esperienza in giappone!
Ringrazio anche il Dr. Gabrio Valotto, per l'aiuto con l'IBIL, e Paolo Franceschetti per le chiacchierate in giardino e per avermi sopportato durante la permanenza nell'ufficio del Prof. Gonella. Grazie anche a "Jimmy" per le pause caffè e le cicchette scroccate e ai miei compagni di corso per l' aiuto e per i tanti momenti divertenti passati in questi anni!
Un grazie di cuore anche al il Prof. Antonio Grandieri, mio professore di fisica delle scuole superiori, che ha sempre saputo consigliarmi per il meglio e del quale ammiro la dedizione e la grande passione per la scienza che riesce a trasmettere.
Se sono arrivato fin qui devo anche ringraziare tutti i "fioi" di Jesolo, per i momenti di svago, per il supporto umano e per l'affetto dimostrato nei miei confronti! Grazie a tutti!!
Un enorme ringraziamento va ai miei genitori e a mio fratello: grazie per avermi permesso di iniziare e concludere al meglio questo ciclo di studi, con i vostri preziosi consigli e aiuti, e con il vostro affetto non mi avete mai fatto mancare nulla.
Infine l'ultimo (ma forse primo per importanza) va ad Aurora, colei che fin dal primo giorno in cui ci siamo conosciuti mi è sempre stata vicino e che quotidianamente, con il suo amore, mi supporta.